Stress field evolution in the northwest Himalayan syntaxis, northern Pakistan

Arnaud Pecher, L. Seeber, Stephane Guillot, François Jouanne, A. Kausar, M. Latif, M. Majid, Gweltaz Mahéo, Jean-Louis Mugnier, Yan Rolland, et al.

Stress field evolution in the northwest Himalayan syntaxis, northern Pakistan

A. Pêcher,[1] L. Seeber,[2] S. Guillot,[1] F. Jouanne,[3] A. Kausar,[4] M. Latif,[4] A. Majid,[4] G. Mahéo,[5] J. L. Mugnier,[3] Y. Rolland,[6] P. van der Beek,[1] and J. Van Melle[1]

Received 21 December 2007; revised 17 July 2008; accepted 11 September 2008; published 3 December 2008.

[1] We have conducted a systematic inversion of striated fault planes throughout northern Pakistan in order to better depict the temporal and spatial variations in stress patterns. Two domains are evidenced at a regional scale, separated by the active Raikhot fault, the western boundary of the Nanga Parbat spur. West of this fault, a wrench-type stress field with $\sigma 1$ axis oriented around N–S predominates in the Karakorum and in Kohistan. It predates Pliocene-Quaternary exhumation of Nanga Parbat and corresponds to the Miocene or earlier regional stress field related to Indian-Asian convergence. East of the Raikhot fault, compression parallel to the belt accounts for initiation of the Nanga Parbat anticlinorium after 5 Ma. It is followed by predominant post-2 Ma extension, both parallel to the belt and NNE–SSW oriented. Thus, in the N–W Himalayan syntaxis, multidirectional extension is juxtaposed on short timescales to shortening either parallel or perpendicular to the belt. Such juxtaposition could be characteristic of strain and stress partitioning during oblique convergence. **Citation:** Pêcher, A., et al. (2008), Stress field evolution in the northwest Himalayan syntaxis, northern Pakistan, *Tectonics*, *27*, TC6005, doi:10.1029/2007TC002252.

1. Introduction

[2] The Himalayan syntaxes have attracted significant attention in recent years because they provide strong indications for coupling between tectonic and surface processes responsible for extremely rapid exhumation documented in the Nanga Parbat (in the NW syntaxis) and Namche Barwa (SE syntaxis) massifs, respectively [e.g., *Zeitler et al.*, 2001a, 2001b; *Burg et al.*, 1998]. Less attention has been paid, however, to the tectonic evolution of these regions, and in particular how stress and strain fields evolved to produce the highly complex, noncylindrical structural patterns observed today. In particular, if tectonics and surface processes strongly interact in these regions, we may ask the question whether (and if so, how) this interaction is recorded by the evolving regional stress fields.

[3] Neotectonic activity in the NW Himalaya has been dramatically emphasized by the recent M = 7.6 Balakot earthquake in Kashmir (8 October 2005). The Balakot earthquake followed the Pattan 1974 earthquake, the epicenter of which was located 100 km farther NW. The focal mechanisms of both earthquakes reveal active thrusting in a NE–SW shortening regime, perpendicular to the average orientation of northwestern Himalaya. A few tens of km farther north, in contrast, a recent microseismicity survey has revealed an active E–W extensional regime in the Nanga Parbat area, while the adjacent Kohistan block appears to be nearly aseismic [*Meltzer et al.*, 2001]. Such a juxtaposition of different tectonic regimes underlines the complex stress and strain pattern in this part of Himalaya: the northwestern Himalaya-Karakorum belt is a typical case of a mountain chain formed by transpressional tectonics, in which strain partitioning has probably controlled the Pliocene-Quaternary tectonics [*Seeber and Pêcher*, 1998], and where exhumation patterns and its driving forces have varied temporally and spatially [*Zeitler*, 1985].

[4] In order to better depict the temporal and spatial variations in stress patterns, we have conducted a systematic inversion of striated faults planes observed in outcrops throughout the northern Pakistan Himalaya. We collected data in a broad area of northern Pakistan, from the Hunza, Gilgit and Indus valleys in the west, to Deosai and Skardu area in the east, and Jhelum valley in the south (Figure 1). Our results complete a preliminary study in the same area [*Pêcher and Seeber*, 2003] and broaden the local investigations of *Zeilinger et al.* [2000] in the southern part of the Kohistan arc along the Indus valley and *Burg et al.* [2005b] in the Kashmir syntaxis.

[5] As compared to similar but older mountain belts, the NW Himalaya seems particularly propitious to such an analysis: to a large extent, inferred paleostress tensors should reflect the recent stress field, as in several areas (i.e., Karakorum, Nanga Parbat, Kashmir) brittle deformation is superimposed on a ductile deformation pattern acquired during early Pliocene times, or possibly even later. In these areas, the paleostress pattern should be similar to the current stress field, which allows some direct control of

[1] Laboratoire de Géodynamique des Chaînes Alpines, CNRS, Université de Grenoble, Grenoble, France.
[2] Lamont-Doherty Earth Observatory, Earth Institute at Columbia University, Palisades, New York, USA.
[3] Laboratoire de Géodynamique des Chaînes Alpines, CNRS, Université de Savoie, Le Bourget du Lac, France.
[4] Geological Survey of Pakistan, Islamabad, Pakistan.
[5] Laboratoire de Sciences de la Terre, CNRS, Université de Lyon 1 et École Normale Supérieure de Lyon, Villeurbanne, France.
[6] Géosciences Azur, UMR 6526, CNRS, Université de Nice, Nice, France.

0278-7407/08/2007TC002252

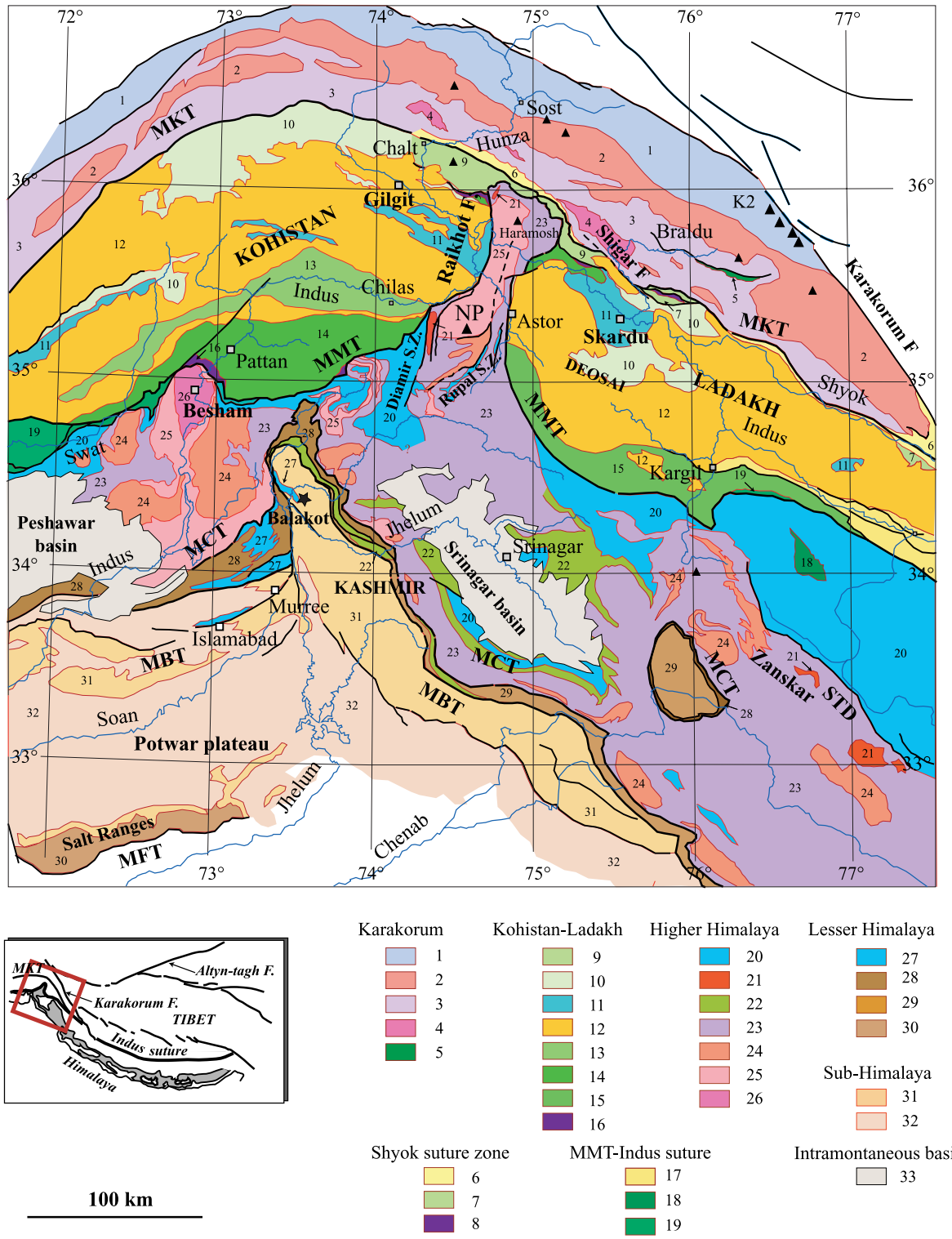
72°
73°
74°
75°
76°
77°
36°
35°
34°
33°
MKT
KOHISTAN
Raikhot F.
Shigar F.
Karakorum F.
Sost
Hunza
Chalt
Gilgit
Haramosh
Baltoro
K2
Braldu
Chilas
Indus
NP
Astor
Skardu
MMT
Pattan
Dianmir S.Z.
Rupal S.Z.
DEOSAI
LADAKH
Shyok
Indus
Besham
Swat
Kargil
Peshawar basin
Indus
Balakot
MCT
Jhelum
Srinagar
Srinagar basin
KASHMIR
Murree
Islamabad
MBT
Soan
Potwar plateau
Zanskar STD
Jhelum
Salt Ranges
MFT
Chenab
MKT
Altyn-tagh F.
Karakorum F.
TIBET
Indus suture
Himalaya
100 km
Karakorum
Kohistan-Ladakh
Higher Himalaya
Lesser Himalaya
Sub-Himalaya
Shyok suture zone
MMT-Indus suture
Intramontaneous basins

Figure 1

the results, and could give a picture of the stress field responsible for the present-day seismicity. In contrast, zones that have apparently been stable since a long period (e.g., Deosai or Kohistan) could have kept traces of older (pre-Pliocene) stress patterns.

2. Tectonic and Morphologic Framework of Northern Pakistan

[6] At a broad scale, the Himalayan mountain belt can be divided into two segments separated by the Karakorum fault, a 1000-km-long right-lateral shear zone, active at least since 21 Ma until 4 Ma [*Valli et al.*, 2007]. Slip rate estimate averaged on the Pleistocene to present time period is 15 to 30 mm a^{-1} [*Armijo et al.*, 1989; *Avouac and Tapponnier*, 1993]. East of this fault, the WNW–ESE to W–E strike of the central and eastern Himalaya is nearly perpendicular to the mean orientation of continent-continent convergence [e.g., *Bendick and Bilham*, 2001; *Paul et al.*, 2001]. Shortening is absorbed mainly by large thrusts and folds striking parallel to the belt, and structures are predominantly cylindrical. West of the Karakorum fault, in contrast, the NW Himalaya (including most of Indian Ladakh and northern Pakistan) has an average NW–SE strike, oblique to Indian-Asian convergence. This obliquity induces a complex strain pattern, in which shortening orientations perpendicular and parallel to the belt are juxtaposed or superimposed, while a large amount of displacement is absorbed along strike-slip shear zones.

[7] A central element of the NW Himalaya is the Kohistan-Ladakh Arc complex, which separates Indian and Asian plate rocks (Figure 1). The Kohistan-Ladakh arc collided with the Asian margin prior to 75 Ma, and was later partly obducted onto the Indian margin [*Coward et al.*, 1987]. It now forms a piece of arc crust, characterized by basic-intermediate rocks, pinched between the Karakorum and Himalayan continental crusts. The Karakorum series have been thrust onto the Cretaceous-Tertiary back-arc formations of the Shyok suture zone [*Sharma and Gupta*, 1978; *Robertson and Collins*, 2002] along the Main Karakorum Thrust (MKT). Along the MKT, north-south shortening structures, prior to 40 Ma, are overprinted by poorly dated dextral strike-slip displacement, combined to SE directed overthrusting [*Coward et al.*, 1986]. In its turn, the Kohistan-Ladakh arc has been thrust southward over the Indian crust along the Main Mantle Thrust (MMT) [*Tahirkheli et al.*, 1979; *Tahirkheli*, 1982], and the Indian crust has been thickened by thrusting along the Miocene Main Central Thrust (MCT), the post-Miocene Main Boundary Thrust (MBT) and the currently active Main Frontal Thrust (MFT).

[8] The most complete tectonic and metamorphic evolution of the NW Himalaya is recorded within the Karakorum series (i.e., north of the MKT, on the Asian side of the belt). Here metamorphism started early, probably before 64 Ma, followed by a distinct event around 44 Ma [*Searle et al.*, 1999; *Fraser et al.*, 2001]. The main metamorphic phase M1 [*Rolland et al.*, 2001, 2006] ended before emplacement of the Baltoro granite at 21 Ma [*Parrish and Tirrul*, 1989], but thrust-driven stacking of the units was active up to 16 Ma, as dated by metamorphic monazites in the Hunza valley [*Fraser et al.*, 2001], and possibly up to 9 Ma, as indicated by Ar-Ar ages of muscovite in thrust-related schistosity in the Chogo Lungma area [*Villa et al.*, 1996]. Same age crustal melting at depth is attested by the Sumayar leucogranite dated at 9.2 Ma [*Fraser et al.*, 1999]. Fission track [*Poupeau et al.*, 1991] and Ar/Ar [*Krol et al.*, 1996] age profiles east of the Hunza valley in the central Karakorum reveal rapid exhumation ($\sim$3 mm a^{-1}) between 20 and 12 Ma, followed by much slower rates (0.7 mm a^{-1})

Figure 1. Geological map of the NW Himalaya. Main tectonic boundaries: MKT, Main Karakotum Thrust; MMT, Main Mantle Thrust (Indus Suture Zone); STD, South Tibetan Detachment; MCT, Main Central Thrust; MBT, Main Boundary Thrust; MFT, Main Frontal Thrust. Geological units, from north to south: Unit A Karakorum: 1, northern sedimentary belt; 2: axial batholith and other granitoids; 3, southern metamorphic belt; 4, felsic gneiss; 5, greenstone complex, Paleozoic (Masherbrum complex). Unit B Shyok suture zone: reactivated along the MKT, 6, predominantly terrigeneous formation; 7, melange zone, predominantly volcanics; 8, ultramafics (Shyok and Dobani-Dassu lineament). Unit C Kohistan: 9, Eocene Chalt (Kohistan) and Kardung (Ladakh) volcanics, Turmik volcanosediments; 10, undifferentiated volcanosedimentary group; 11, metasediments; 12, plutonic rocks (Kohistan and Ladakh batholith); 13, gabbronorites (Chilas complex); 14, southern amphibolites (Kohistan); 15, Dras volcanosedimentary group (Ladakh); 16, mantle ultrabasites (Jijal complex). Unit D MMT-Indus suture zone: 17, Indus molasses; 18, Spontang ophiolites; 19, imbricate thrust units, with blue schists. Unit E Higher Himalaya: 20, Neotethyan sedimentary group (Permian-Eocene); 21, Tertiary leucogranites (Ladakh and Nanga Parbat); 22, Panjal Traps (Permian); 23, High Himalaya Crystalline (mainly metasediments, Late Proterozoic to early Paleozoic); 24, Paleozoic intrusives (Swat and Manserah granite, Kohistan, Bhazum and Kade granite, Ladakh); 25, basement gneiss (dominantly Early Proterozoic orthogneiss); 26, Besham metaigneous. Unit F Lesser Himalaya: 27, Paleozoic-Eocene cover; 28, upper nappe, dominantly Early Proterozoic metasediments (Abbottabad, Kishtwar); 29, lower nappe, dominantly Late Proterozoic–Paleozoic metasediments (Kishtwar, Kashmir); 30, Salt Ranges (Late Proterozoic–Eocene Indian cover). Unit G Sub-Himalaya: 31, Muree and Subatu formations (Eocene to Miocene); 32, Siwaliks (middle Miocene to Quaternary); 33, Peshawar and Srinagar intramontaneous basins (Quaternary). Personal data and modified from *Bossart and Ottiger* [1989], *Burbank et al.* [1986], *Greco et al.* [1989], *Burg et al.* [2005a], *DiPietro et al.* [2000], *DiPietro and Pogue* [2004], *Edwards et al.* [2000], *Fontan et al.* [2000], *Gaetani* [1997], *Greco* [1991], *Kasmi and Jan* [1997], *Le Fort and Pêcher* [2002], *Lombardo and Rolfo* [2000], *Reuber* [1989] *Rolland et al.* [2000, 2002], *Schneider et al.* [2001], *Steck* [2003], *Tahirkheli* [1996], *Valdiya* [1998], *Wadia* [1975], and *Zanchi and Gaetani* [1994].

from 6.6 to 2.4 Ma. Strong Mio-Pliocene and Quaternary tectonic reactivation, accompanied by rapid exhumation of middle and lower crustal rocks, led to the present-day relief of Karakorum, characterized by high summits with altitudes reaching >7500 m, strong incision of rivers that cut down to altitudes <2000 m, and steep slopes. Tectonics appears mainly active in the eastern Karakorum, where the highest peaks of the NW Himalaya occur (with five peaks over 8000m, among which K2, 8611 m). Here, Neogene tectonism is manifested by a series of dome-shaped anticlines aligned along the east–west Braldu line [*Bertrand et al.*, 1988; *Rolland et al.*, 2001]. In the domes, most low- and intermediate-temperature thermochronological systems record Plio-Pleistocene cooling ages, revealing recent rapid exhumation from midcrustal depths. The domes initially grew as transpressional folds, initiated in a tectonic corridor bounded by two NW–SE faults [*Pêcher and Le Fort*, 1999; *Rolland et al.*, 2001; *Mahéo et al.*, 2004]: the major and currently active Karakorum fault to the NE, along which the highest peaks are lined up, and the parallel Shigar fault to the SW (Figure 1). The latter fault should have a recent vertical offset of more than 2 km, but we have not been able to find any indication of late Quaternary activity in the field. The domes evolved by rapid diapiric amplification within migmatized anticline cores, with exhumation rates attaining 5.5 mm a^{-1} from 6.7 to 4.7 Ma (Ar-Ar cooling ages ranging up to 4.7 Ma [*Searle et al.*, 1989]), and were finally exposed during E–W buckling and uplift of the whole southeast Karakorum [*Mahéo et al.*, 2004].

[9] South of the MKT, the Kohistan Arc formations crop out in two broad blocs on each side of the Nanga Parbat spur, Kohistan to the west and Ladakh to the east, linked north of the Nanga Parbat by a thin strip of arc volcanites and metasediments. Kohistan and Ladakh have been free of Miocene or younger reactivation. They have a similar average elevation as adjacent high-relief areas of Karakorum and Nanga Parbat, but with a much smoother relief. The most striking example of such high-elevation, low-relief areas is the Deosai plateau in Pakistani Ladakh, a conspicuously flat plateau at around 4000 m elevation between the Nanga Parbat massif to the west, the Indus valley to the north and the Shigar valley to the east. Recently acquired low-temperature thermochronology data from the Deosai plateau indicate slow exhumation between 40 and 20 Ma, bracketed by zircon (U-Th)/He, and apatite FT and (U-Th)/He ages [*Van Melle et al.*, 2007]. The recorded slow and continuous exhumation implies that the plateau probably attained its modern morphology already long before 20 Ma.

[10] Between Kohistan and Ladakh, the Nanga Parbat–Haramosh spur corresponds to a crustal-scale, N–S elongated dome [*Schneider et al.*, 2001] exhuming a window of Himalayan gneisses from below the Kohistan arc rocks of the MMT hanging wall. In the Nanga Parbat area, the MMT has been refolded into a broad N–S anticline. Because of this fold, ductile mylonites related to the MMT crop out on both sides of the Nanga Parbat spur in two shear zones, with apparent right-lateral (eastern side) and left-lateral (western side) movements, respectively [*Edwards et al.*, 2000]. In the Nanga Parbat gneisses, Ar-Ar cooling ages on biotite range from 5 Ma in the limbs of the fold to 1 Ma in its core [*Schneider et al.*, 2001], with intrusive leucogranite lenses as young as 1.4 Ma [*Zeitler et al.*, 1993]. West of the fold, the Raikhot fault reactivates the MMT and Diamir shear zone. Along this fault, the western limb of the Nanga Parbat overthrusts Pleistocene Indus alluvial terraces [*Butler and Prior*, 1988]. Together with the strong relief [*Burbank et al.*, 1996], similar to the Karakorum, the distribution of the Pliocene-Quaternary cooling ages, and the earthquake focal mechanisms (Figure 2), evidence the fast amplification of the fold from upper Miocene up to present, as a pop-up anticline [*Edwards et al.*, 2000] exhuming in a regime of east–west shortening.

[11] Southwest of Nanga Parbat, the Besham syntaxis (Figure 1) also corresponds to a N–S trending anticline. It indicates a similar origin as for Nanga Parbat but at a less evolved stage. In this area, *Zeilinger et al.* [2000] have proposed a complex tectonic history, inferring from the inversion of fault data the probable superposition of three different stress fields since late Miocene times.

[12] South of Nanga Parbat, the southern Himalayan accretionary prism constitutes a fold-and-thrust belt involving the MCT, the MBT and the MFT. It is a region of intermediate relief, juxtaposing flat basins such as the Peshawar and Shrinagar basins and the Potwar Plateau (Figure 1) with zones marked by active erosion, deep valleys, steep sidewalls, but no high summits. The tectonic pattern is complex, mimicking the one observed farther north in Nanga Parbat. After southward thrusting of the Lesser Himalayan formations onto Miocene series along the MBT, the entire pile was refolded in a north–south trending anticline, which provides evidence for E–W shortening. Earthquake focal mechanisms, in contrast, indicate active NE–SW shortening, perpendicular to the regional trend of the NW Himalaya (Figure 2).

[13] In summary, the northwest Himalayan syntaxis displays a present-day geological pattern made of a puzzle of clearly identifiable large blocks, with contrasting evolutions. Some areas are apparently passive since Miocene, while some others reveal active Pliocene-Quaternary ductile tectonics. The timing of brittle deformation should thus be different from one block to another. In the zone of recent exhumation (Karakorum dome, Nanga Parbat), it can be roughly bracketed using Ar/Ar cooling ages: the closure temperature for biotite is commonly quoted as 300 ± 50°C [e.g., *Harrison et al.*, 1985; *MacDougall and Harrison*, 1999], although it might be significantly higher depending on chemical composition [*Grove and Harrison*, 1996]. This temperature is 150° lower than the currently accepted temperature for the ductile-brittle transition in the crust (300–450°C) [*Scholz*, 1988, 2002; *Viganò and Martin*, 2007], thus the change from ductile to brittle deformation should be slightly older than the biotite ages. Nevertheless, in areas of rapid cooling and exhumation, this time discrepancy will be small (typically $\leq$ 1 Ma). Accordingly, brittle deformation in the Karakorum domes or the Nanga Parbat anticline should be mainly late Pliocene or Quaternary in age. In contrast, in Kohistan and Ladakh (particularly on the

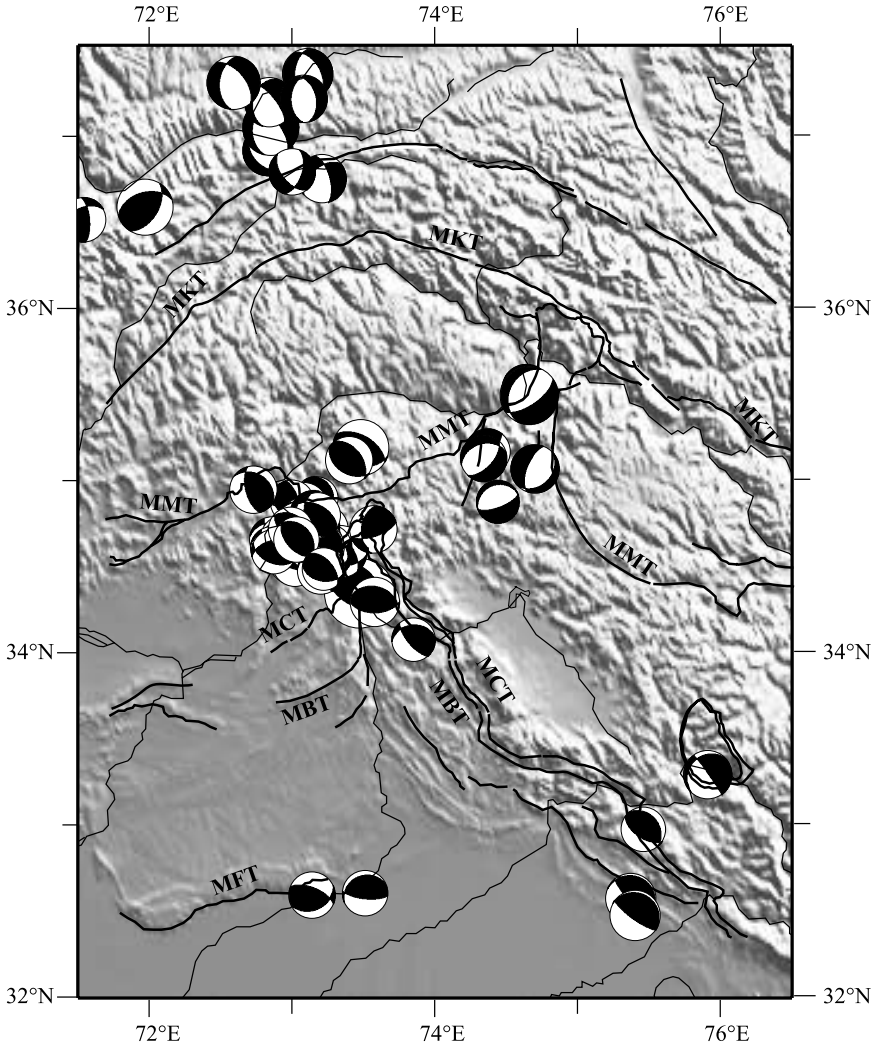

Figure 2. Focal mechanism solutions in NW Himalaya, CMT solutions. White indicates P axis quadrant, black indicates T axis quadrant. See Global CMT Web page http://www.globalcmt.org/.

Deosai Plateau, already cooled 20 Ma ago), one can expect the fault data to retain a memory of the stress state prior to Miocene-Quaternary exhumation of Nanga Parbat and Karakorum, even if older brittle faults in those areas could have been reactivated during these late events. In the Siwaliks formations, the main deformation phase is post-Miocene, as evidenced by the folding of the Tertiary Siwalik series, together with the MCT and the MBT, in sharp N–S trending folds in the Kashmir syntaxis. The timing of the brittle deformation is currently poorly constrained. *Burg et al.* [2005b] provide evidence from fault analysis for two successive paleostress orientations, with predominant NE–SW and E–W compression, respectively. Their relative chronology remains unknown. Nevertheless, we note that E–W compression is coherent with the east–west shortening evidenced by the folding of Miocene series and MBT in the Hazara Kashmir syntaxis, while NW–SE compression fits with the focal mechanisms and displacements deduced from earthquakes (Figure 2).

3. Methodology

[14] Several methods have been developed to use sets of fault planes and slickenlines with kinematic indicators to depict paleostress tensors. Most of them are based on the concept of the reduced stress tensor; that is, they aim to determine the orientation of the principal stress axes $\sigma1$, $\sigma2$, $\sigma3$ (with $\sigma1 \geq \sigma2 \geq \sigma1$ and compression being positive) together with a shape parameter. The shape parameter can be either *Lode*'s [1925] parameter $\mu = (2\sigma2 - \sigma1 - \sigma3)/(\sigma1 - \sigma3)$, *Bishop*'s [1966] parameter $\Phi = (\sigma2 - \sigma3)/(\sigma1 - \sigma3)$ [e.g., *Angelier*, 1975, 1979, 1984; *Yamaji*, 2000], or the similar parameter $R_0 = (\sigma1 - \sigma2)/(\sigma1 - \sigma3)$ [e.g., *Célérier*, 1995; *Zeilinger et al.*, 2000; *Burg et al.*, 2005b]. All inversion methods rely on several assumptions: (1) the

stress is uniform over the volume where the fault data for the inversion are measured; (2) the stress tensor is equivalent to the incremental deformation tensor, as obtained from the slip data; and (3) the basic hypothesis of *Bott* [1959], which considers that the slip vector on a plane, as given by the slickenlines in the case of striated fault planes, is parallel to the maximum shear stress along the fault plane as deduced from the stress tensor. Because of the nonideal conditions (for instance, guided movement of the various blocks cut by the faults, non infinitesimal displacements, etc.), some discrepancy is accepted. The quality of the inversion is estimated from the angular misfits between theoretical striae predicted from the calculated tensor and the measured striae.

[15] In the case of an area where the amount of deformation is small and all fault movements observed at a given scale (typically on an outcrop of a few tens of square meters) result from a uniform stress field, direct inversion by purely analytical means (i.e., a search of the tensor which minimizes angular misfits, as proposed, for instance, by *Angelier* [1975]) yields similar stress parameters regardless of the methods. In such cases, a good preliminary estimate of the orientation of the stress axes can in fact usually already be given in the field from observations of conjugate fault sets, and the numerical stress inversion mainly adds the shape parameter of the stress ellipsoid.

[16] In most natural cases, however, the observed brittle structures record a complex tectonic history, with superposition of several stress states in the same area. When dealing with the resulting heterogeneous fault slip data (i.e., where not all faults slipped in response to the same deviatoric stress, and where newly formed faults are combined with reactivated fractures), separation of stress tensors becomes a challenging target. The problem has been addressed in several ways. It is possible to separate subsets of faults from the data set, based on geological considerations: for instance, evidence of reactivation of faults, with crosscutting relationships or superimposition of striae; separation of fault sets based on differences in mineral coatings; or in case of an assumed Andersonian geometry (one of the principal stress orientations approximately vertical and the other two horizontal), a priori separation of normal and transtensional faults (corresponding to horizontal extension) from reverse or transpressional faults (horizontal shortening). Alternatively, semiautomatic or automatic approaches attempt to extract the set of tensors that best fits the given set of faults, independent of geological criteria. In semiautomatic methods, a first tensor is computed, which minimizes the sum of the angular misfits. The method is then applied recursively to subsets of the data that show large misfits from slip directions predicted from formerly determined stress tensors [e.g., *Etchecopar et al.*, 1981; *Armijo et al.*, 1982]. Automatic determination of the tensor can also be based on statistical techniques of cluster analysis (see *Nemcok and Lisle* [1995], who group the faults in dynamic subsets prior to normal stress inversion). In multiple inverse methods [*Yamaji*, 2000; *Otsubo et al.*, 2006], significant solutions calculated on small subsets of faults are identified as clusters in the parameters space. Whatever the method, however, it appears that inversion of heterogeneous fault slip data cannot be fully automated and implies "researcher decisions" [*Liesa and Lisle*, 2004].

3.1. Measuring the Data

[17] Altogether, we have measured more than 2800 fault/striation pairs from 120 sites (Figure 3 and Table S1 in the auxiliary material),[1] spread from the Salt Ranges to the northern Karakorum. Each site corresponds to between 8 and 43 measurements (generally around 25) on a single outcrop or on a section no longer than 50 m. The quality of measurement was noted (in particular the degree of confidence in the inferred sense of movement); where the quality was weak (usually because of an unclear sense of movement), the fault was either rejected or labeled as suspect. The presence and nature of crystallization on the fault plane was noted in order to attempt to separate sets of different ages, but no clear general distinction has resulted from this sorting.

[18] Most of our measurement sites are along fresh road cuts. On such sections, an exhaustive view of all faults is easy to obtain, while it is often difficult to find sufficient faults and good quality movement criteria in natural outcrops. Accordingly, our network of stations is irregularly spaced: it is dense in the Nanga Parbat–Haramosh area, which is traversed by the Karakorum Highway, the Skardu road and the Astor-Deosai road, but sparser within the Karakorum Range and nearly empty in the southern part of Nanga Parbat, which is a restricted area close to the India-Pakistan Line of Control. Only a few sites have been measured along the Karakorum Highway in the Pattan area, where the MMT forms a north–south trending fold suggesting a growing (or aborted) structure similar to Nanga Parbat. This section has been studied in detail by *Zeilinger et al.* [2000]. Farther south, in the southern Himalayan fold-and-thrust belt (Hazar-Kashmir syntaxis and frontal Salt Ranges), propitious outcrops are scarce. We have measured only about 10 sites, which augment the data obtained by *Burg et al.* [2005b]. Thus we can compare results obtained using different inversion methods (inversion with the FSA software of *Célérier* [1995] for the previous authors, multiple inverse method of *Yamaji* [2000] for this study).

3.2. Processing the Data

[19] In most of the measurements sites, faults orientations are dispersed, and faults cannot be easily grouped in subsets based on geological criteria. There are numerous indications for superimposition of movements, but relative chronology criteria are rare and often ambiguous (for instance, several tests on planes with superposed striae show that the relative chronology is subject to observer bias). Therefore, in most cases the separation of fault subsets in the field prior to their numerical treatment was at best unclear, and the determination of the relative chronology of the tensors based on local geological criteria mostly unsuccessful.

[1] Auxiliary materials are available in the HTML. doi:10.1029/2007TC002252.

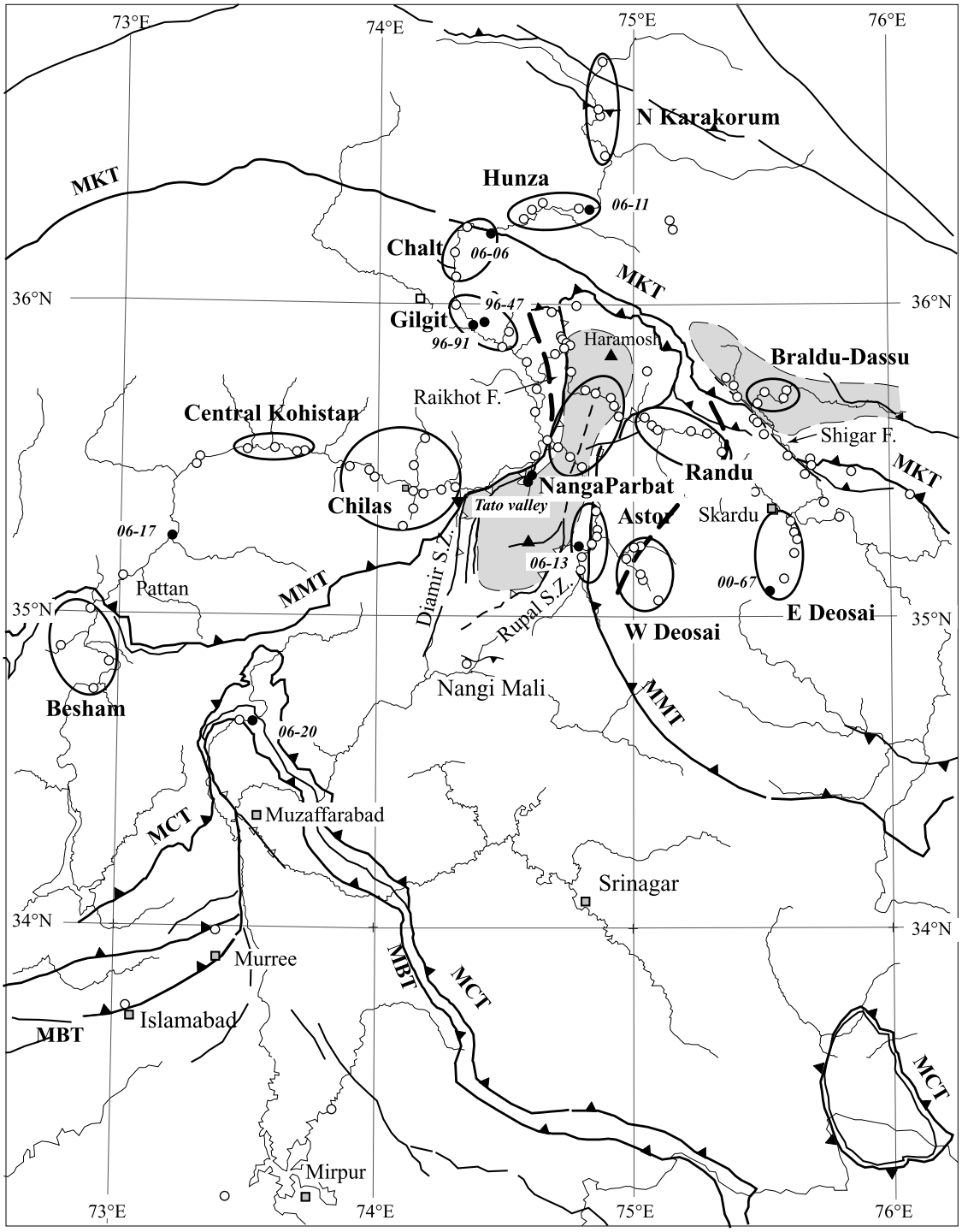

Figure 3. Localization of the fault stations (plain dots) and identification of the grouped sites. Black symbols and reference numbers indicate sites referred to in the text (see Figures 6 and 9). Shaded area indicates zones of Plio-Quaternary very active exhumation (core of the Nanga Parbat pop-up anticline, SE Karakorum domes). Thick dotted line indicates Nanga Parbat morphological limit.

[20] Accordingly, we have favored a mainly automatic approach for treating our data. We used the multiple inverse method, as developed in the software package mim5-miv4 of A. Yamaji et al. (Multiple Inverse Method Software Package, Freeware package, 2005, http://www.kueps.kyoto-u.ac.jp/~yamaji/PDS/indexe.html). The method is based on the direct determination of stress tensors on all small subsets of faults (typically 4 to 6 faults) that can be extracted from the given larger set of measurements collected in a station. The method uses a

computational grid of 60,000 points, the optimal stress being approximated by the nearest grid point. Points of the grid with a significant number of solutions tied to it are plot in a stereogram. Significant stresses will be revealed on the stereogram by clusters of solutions sharing a similar shape ratio. According to *Liesa and Lisle* [2004], this method achieves good solutions under general conditions, provided that the number of faults in the different subgroups leading to the determination of the different tensors is similar; minor stress tensors are difficult to detect.

[21] To process the data, we followed a multistep approach, similar to that of *Zeilinger et al.* [2000]: in areas were our network of sites was sufficiently dense, we have attempted to average the regional stress field at a scale of a few tens of kilometers by grouping the sites located in a geologically and tectonically homogeneous unit, and processing them as a single site (Figure 3). In the case of a heterogeneous stress field (due to superposition of several tensors), the large number of faults considered allows a more robust determination of the tensors, each tensor being calculated on a large subset of faults. To illustrate our approach, we will treat the example of the Gilgit area in some detail below. Data from each station were subsequently individually processed.

[22] Finally, for interpretation and discussion of the results we define ''tilted'' and ''untilted'' tensors. Whatever the tectonic regime (compression, wrench or extension), it is generally assumed, following Andersonian fault theory, that one of the principal stress orientations is approximately vertical and the other two horizontal [*Célérier*, 1995]. In fact, we often obtain both ''untilted'' tensors (tensors for which one main axis is close to vertical and the other two close to horizontal) and ''tilted'' tensors (for which none of the main axes is close to vertical) in a single site. In a region such as northern Pakistan, with a complex tectonic history and strongly contrasted topography, the latter can be due to relief effects, or can correspond to tensors calculated on faults rotated during later movements. We will base our interpretation of the results largely on the main stress orientations of the ''untilted'' tensors.

3.3. Using the Multiple Inverse Method: Example of Gilgit Area

[23] In the Gilgit area, we have collected data at five different sites, spread in a sector of 25 km along the Hunza and Gilgit rivers (Figure 3). All measurements were taken in dioritic rocks (Dainyor diorite) of the northern Kohistan Arc, south of the lineament of ultramafic rocks that separates the predominantly plutonic central Kohistan region from the northern volcano-sedimentary series (Figure 1) [*Le Fort and Pêcher*, 2002]. When merged together, these provide a set of 110 fault measurements from a tectonically and lithologically homogeneous area.

[24] Figure 4 shows the whole set of data projected in a Wulff net. A wide dispersion of fault orientations can be seen, suggesting a multisteps brittle deformation story. The plot clearly shows mixing of positive and negative rake values for striae of similar orientation, which implies superposition of different stress states, possibly including stress axis inversion. When considering the histograms of fault strikes and dips (Figure 4), a preferred orientation of the faults (strike mode around 210° and dip mode around 60°, i.e., steeply westward dipping faults) clearly appears, but the histogram of rakes again illustrates the great heterogeneity of movements.

[25] To search for best fitting stress tensors, we use the miv4 software package of A. Yamaji et al. (Multiple Inverse Method Software Package, Freeware package, 2005, http://www.kueps.kyoto-u.ac.jp/~yamaji/PDS/indexe.html). The $\sigma 1$ and $\sigma 3$ orientations obtained for 234 significant fault subsets are plotted Figure 5. Figure 5 shows clustering of the $\sigma 1$ poles around a main orientation (N190°E with a southward plunge), but the Φ ratio is poorly defined. A secondary cluster corresponds to steep $\sigma 1$ orientations. To discriminate possible tensors, we test the quality of the results while increasing the Φ ratio from 0 to 1 with steps of 0.1.

[26] This analysis yields nine possible tensors (Table 1), eight for a gently plunging $\sigma 1$ axis and one for steeply plunging $\sigma 1$. An estimate of the quality of the result is given by the percentage of faults for which the deviation between the measured striae and the theoretical maximum shear stress on the plane (misfit angle α) is less than a given threshold value. As shown by *Liesa and Lisle* [2004], it is the most sensitive parameter to discriminate tensors. Those authors favor a misfit threshold of 12°. Tables 1 and 2 consider misfit thresholds of 12°, 20°, 30° and 45°.

[27] Table 1 shows that similar stress orientations are obtained when increasing the Φ ratio from 0.1 to 0.8 (T1 family, east–west $\sigma 3$ and north–south $\sigma 1$), while a tensor T2 (for $\Phi = 0.8$) has a distinct orientation (east–west $\sigma 3$ and steep $\sigma 1$). A detailed analysis identifies a single subset of faults that controls the calculation for all the tensors of the T1 family. To select the Φ ratio for the T1 tensor, we will rank the T1 solutions according to the number of faults with a striation close to the theoretical shear stress orientation. Accordingly, the tensors with a Φ ratio around 0.4 to 0.6 best fit the data. To better fix the ratio, we recalculate the misfits for intermediate Φ values (the miv4 software allows only 0.1 steps). The largest number of faults compatible with T1 for a threshold of 12° is for $\Phi = 0.38$. Table 1 shows that tensor T2 (for $\Phi = 0.82$) which has an orientation distinct from T1 accounts for a smaller number of faults. The set of faults controlling the T2 tensor is clearly distinct (Table 2), however, and we can accept the T2 tensor as a well-defined distinct tensor. Thus, we can conclude that faults in this area record at least a two-stage brittle deformation history, corresponding to the two stress tensors T1 and T2, even if slips corresponding to T2 are scarce. Additionally, a large amount of fault slips fit neither with T1 nor with T2. This result indicates that additional minor stress deviation must occur but has not been identified.

[28] The same superposition of tensors can be retrieved at the station scale, as illustrated in Figure 6: the two stations 96-91 and 96-47 (Figure 3 for localization) share the same predominant set of steep west dipping faults. In station 96-91, they carry left-lateral strike-slip movements and are

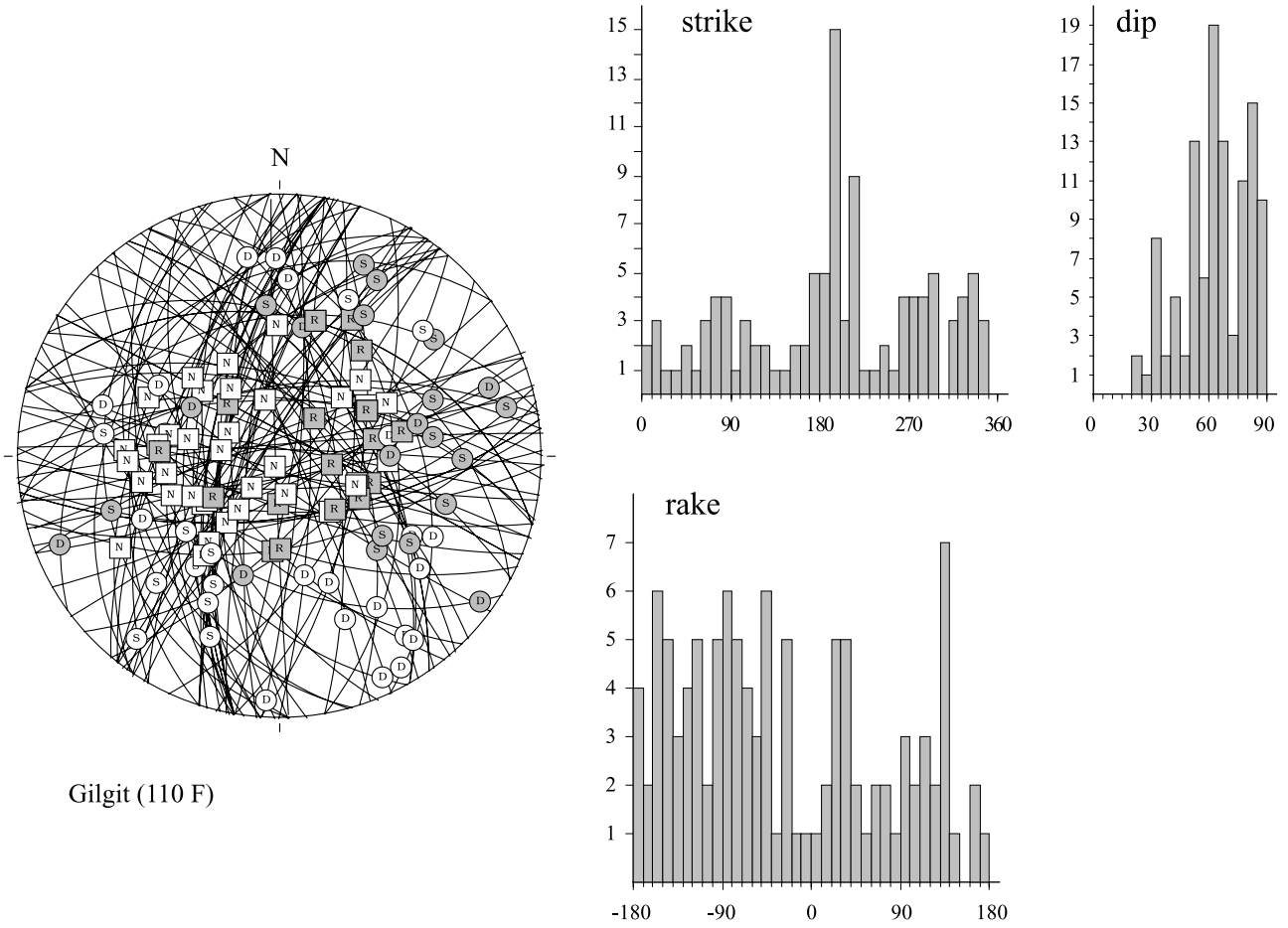

Figure 4. Faults in Gilgit area, northern Kohistan. Set of 110 fault/striation pairs. (left) Stereographic projection, Wulff net lower hemisphere. The sense of movement for each fault is given by the specific symbol used to plot the striae (N, R, S, and D for normal, reverse, sinistral, and dextral faults, respectively). The color of the symbol accounts for the sign of the rake of the slip, the rake λ being defined as the angle between the slip vector of the hanging wall relative to the footwall and the fault plane strike direction, so that $\lambda > 0°$ for reverse faults and $|\lambda| \leq 90°$ for sinistral faults [see *Célérier*, 1995], a gray symbol for positive rake (i.e., movement on the fault has a reverse component, indicating shortening deformation component), and a plain symbol for negative rake (i.e., movement on the fault has a normal component, extensional deformation component). (right) Histograms for fault strike (right-hand rule) and dip values and a histogram for striae rake values. Classes are of 10°.

coupled to a conjugate set of right-lateral faults. The predominant tensor calculated for this station (Table S1 in the auxiliary material) is close to T1 and can account for nearly all the faults. In station 96-47, the majority of the west dipping faults displays normal movements. The predominant tensor is now close to T2, but a large residue of faults (mainly the south dipping reverse faults) is better explained by T1 than T2. In this station, scarce superposition criteria would favor a relative chronology of T1 followed by T2.

4. Results

4.1. Regional-Scale Average Stress Fields

[29] In areas with sufficient sites in a homogeneous structural unit, we have grouped the stations to estimate a regional average stress field. Table 3 reports the results obtained by grouping the stations. It illustrates the wide range of stress tensors required by the data, either within a given area (implying superimposed successive stress states), or from one area to another (implying regional variations of the paleostress field). In Table 3, we have arbitrarily retained only the tensors which misfits less than 30° for at least 30% of the faults (except for Astor and Randu area, where less predominant tensors are needed to explain the data). For each area, two or three tensors are sufficient to explain the majority (up to 80% for Chalt area, 50 to 60% for other areas) of observed fault kinematics. Additional tensors can be calculated to improve the fit, but whatever the number of tensors, we keep a residue of ~10% unexplained fault/striae pairs. Considering the tensors required to decrease the residue (tensors not reported in Table 3) two

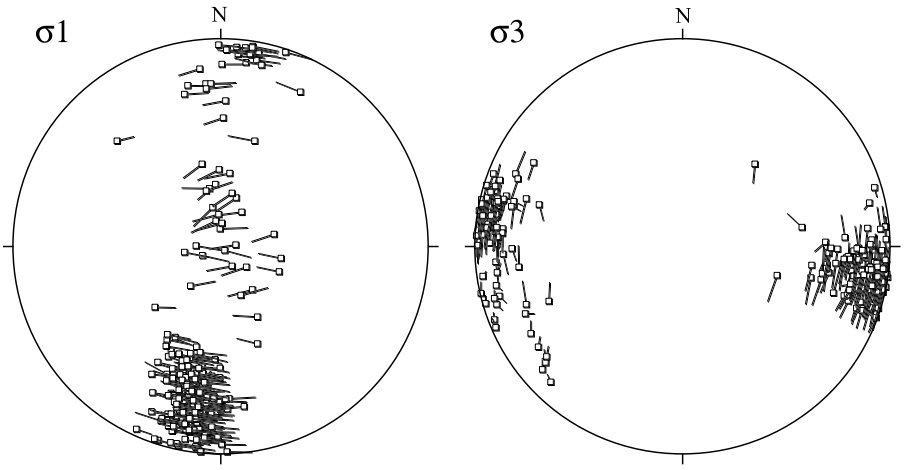

Figure 5. Gilgit area, results from the multiple inverse methods (software package mim5-miv4 of A. Yamaji et al., Multiple Inverse Method Software Package, Freeware package, 2005, http://www.kueps.kyoto-u.ac.jp/~yamaji/PDS/indexe.html); 224 points (from a 60,000 nods grid) having a significant number of $\sigma 1$ or $\sigma 3$ orientations tied to them, plotted lower hemisphere, equal-area projections. (left) Square symbols define the $\sigma 1$ orientations, the bars attached on the squares show the plunge and azimuth of $\sigma 3$ axis (the shorter the lines, the steeper the corresponding stress axes). (right) Squares define $\sigma 3$ orientations; the bars show the plunge and azimuth of $\sigma 1$ axes.

cases are common: (1) they are tensors having different principal stress orientations as compared to the retained tensors but accounting for only a small number of data (we have neglected these) and (2) they are tensors with similar principal stress axis orientations as those reported, but with a different Φ ratio. These probably reflect progressive changes in the strain regime, from compression to wrench or from wrench to extension.

[30] Main results are presented in two ways: using a tectonic regime plot [*Armijo et al.*, 1982; *Célérier*, 1995] and as a map representation of the projections of $\sigma 1$ and $\sigma 3$ orientations onto the horizontal plane.

[31] In the tectonic regime plot (Figure 7), only tensors with one vertical or close to vertical axis (i.e., ''untilted'' tensors) can be plotted. This plot distinguishes extensional, wrench and compressional strain regimes, on the basis of which of the principal stress axes is vertical. West of the Raikhot fault, wrenching is the most common strain regime. It corresponds mainly to steep strike-slip faults. In the Besham, Nanga Parbat and Dassu dome areas, extension (mainly normal faults) is predominant. Extension has also been evidenced in all other main tectonic units. In contrast, records of compressional strain (mainly reverse faults) are rare. The plot also shows the variability of the Φ ratio (varying from 0.1 to 0.8) in a single area (as already demonstrated for the Gilgit test area) or from one area to another. Such variability reveals instability of the stress state, with rapid shifting from one type of stress regime to another through permutation of the $\sigma 1-\sigma 2$ or $\sigma 2-\sigma 3$ axes, for high or low values of Φ, respectively.

[32] The map (Figure 8) shows the main tensor orientations obtained for each area as a horizontal projection of the principal stress axes. For the sake of clarity, only two tensors are shown for each region. In most cases, we

Table 1. Main Tensors Coming Out From the Set of 110 Faults Measured in Gilgit Area[a]

Tensor	Φ	$\sigma 1$	$\sigma 3$	$\alpha < 12°$ (%)	$\alpha < 20°$ (%)	$\alpha < 30°$ (%)	$\alpha < 45°$ (%)
T1	0.1	36/196	14/096	18.2	24.5	31.8	46.4
T1	0.2	41/196	05/101	19.1	26.4	34.5	49.1
T1	0.3	33/195	10/099	22.7	30.9	38.2	51.8
T1	0.4	33/193	00/103	24.5	31.8	42.7	48.2
T1	0.38	33/193	00/103	26.4 (29 f)	31.8	41.8	49.1
T1	0.5	28/193	04/101	23.6	36.4 (40 f)	44.5 (49 f)	50.9
T1	0.6	13/190	02/099	18.2	33.6	40.9	51.8
T1	0.7	19/187	09/280	18.2	30.0	38.2	50
T1	0.8	18/190	10/097	18.2	28.2	40.1	54.5
T2	0.8	78/124	11/277	15.5	24.5	33.6	50
T2	0.82	78/124	11/277	15.5 (17 f)	25.5 (28 f)	33.6 (37 f)	50

[a]Axis orientations given as plunge/plunge direction. For α the percentage of faults for which the misfit angle between the observed and calculated striae is less than 12°, 20°, 30°, and 45°.

Table 2. Number of Fault Movements Measured in the Gilgit Area That Can Be Explained by T1 and T2 or Indifferently by T1 and T2

Misfit Threshold	Fitting Only With T1	Fitting Only With T2	Fitting With Both T1 and T2	Total
<12° (Φ = 0.38)	24 (21.8%)	12 (10.9%)	5 (4.5%)	41 (37.7%)
<12° (Φ = 0.5)	20 (18.2%)	11 (10.0%)	6 (5.5%)	37 (33.6%)
<20°	21 (19.1%)	9 (8.2%)	19 (17.3%)	49 (44.5%)
<30°	21 (19.1%)	9 (8.2%)	26 (23.6%)	58 (52.7%)
<45°	14 (12.7%)	13 (11.8%)	42 (38.2%)	69 (62.7%)

retained the two tensors accounting for the largest number of observed fault movements (Table 3). When these two tensors were nearly parallel and mainly differed by their Φ ratio, we display the most important tensor with significantly different orientation, if any.

[33] A number of features are particularly noticeable in Figure 8. First, the plunge of $\sigma 3$ is predominantly low, that is, wrench or extensional deformation predominates. The predominantly low plunge of $\sigma 3$ axes contrasts with the greater observed variability for the plunges of $\sigma 1$. Second,

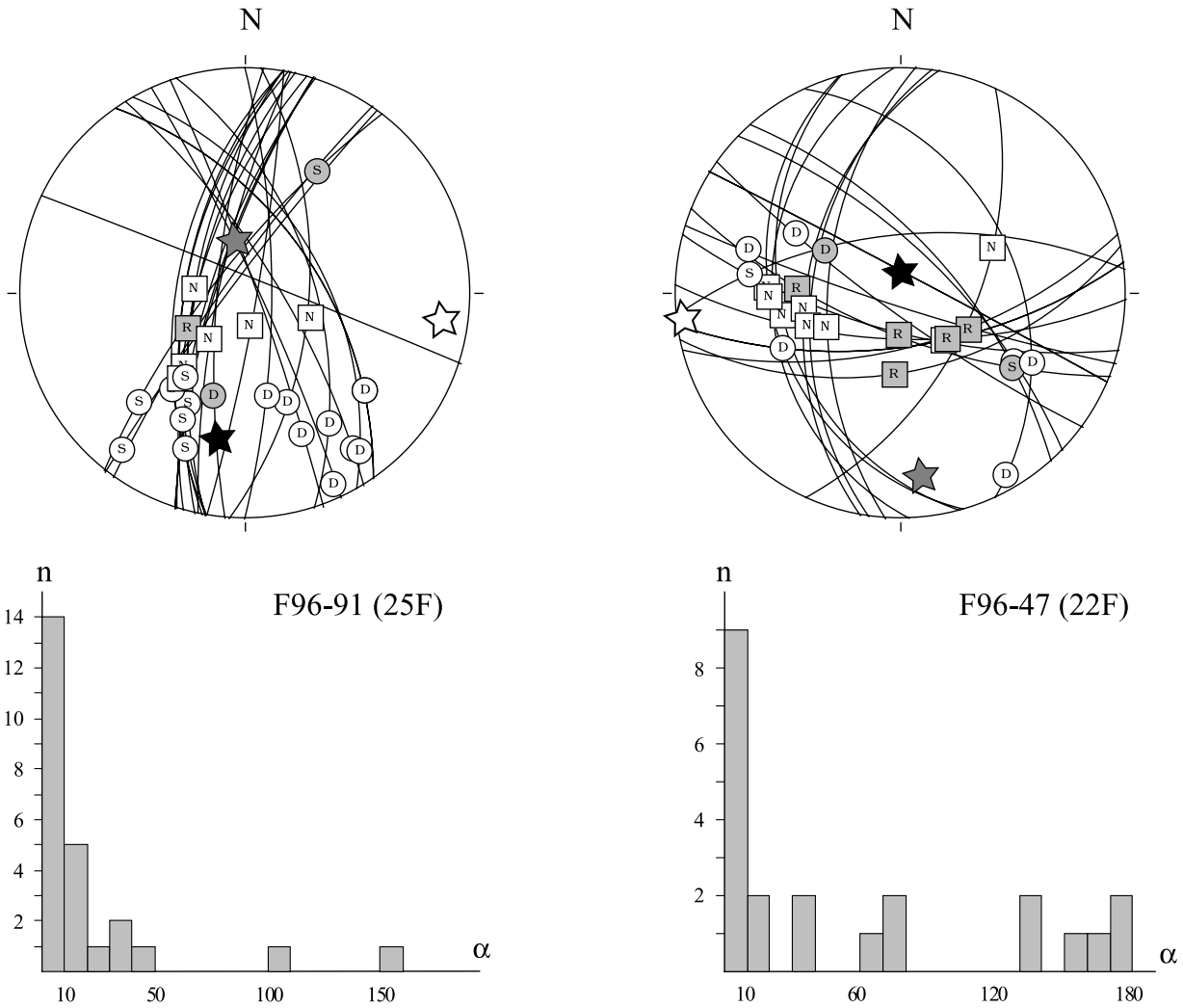

Figure 6. Sites 96-91 and 96-47 from Gilgit area (see Figure 3 for location). Projection of the fault/striation pairs, Wulff net, lower hemisphere (same conventions as Figure 4). Black star and plain star indicate positions of $\sigma 1$ and $\sigma 3$ calculated using the miv4 software package of A. Yamaji et al. (Multiple Inverse Method Software Package, Freeware package, 2005, http://www.kueps.kyoto-u.ac.jp/~yamaji/PDS/indexe.html). Grey star indicates $\sigma 2$. Histograms show misfit angles α between the striae and the theoretical shear stress on the fault, for classes of 10°.

Table 3. Main Tensors Coming Out From Grouped Stations[a]

Tensor	Φ	σ1	σ3	α < 12° (%)	α < 20° (%)	α < 30° (%)	α < 45° (%)
Astor (218F) Nanga Parbat Cover (Metasediments)							
T1	0.07	22/266	33/011	15	22	30	35
T2	0.42	51/272	02/005	16	22	26	34
T3	0.52	83/276	00/006	8	17	24	33
All tensors				26	38	46	53
Besham (88F) Himalayan Gneiss							
T1	0.72	69/219	19/014	17	23	33	42
T2	0.12	76/115	01/207	19	25	31	39
T3	0.55	42/139	31/016	18	24	30	33
All tensors					35	43	50
Central Kohistan (141F) Chilas Gabbro-Norite Complex							
T1	0.82	03/310	24/041	18	29	38	46
T2[b]	0.28	14/344	10/077	21	29	37	44
T3[b]	0.28	06/353	83/199	15	24	31	37
All tensors				39	51	64	71
Chalt (95F) Chalt Volcanics							
T1	0.32	07/038	03/129	28	34	41	47
T2	0.05	00/241	83/149	22	27	37	43
T3[c]	0.25	80/049	10/234	22	28	33	39
All tensors				55	70	80	87
Chilas (241F) Chilas Gabbro-Norite Complex							
T1	0.8	77/124	11/271	20	27	34	44
T2	0.93	06/000	14/269	18	26	34	47
T3	0.75	82/206	08/019	9	15	21	28
T4	0.4	07/252	03/342	8	14	19	25
All tensors				33	46	57	70
Dassu Dome (87F) Karakorum Orthogneiss							
T1	0.18	86/045	04/198	20	33	45	51
T2	0.4	80/199	09/356	17	32	44	48
All tensors				30	46	57	61
Deosai E (160F) Ladakh Plutonites and Volcanites							
T1	0.55	71/108	13/235	16	24	31	37
T2	0.21	51/241	37/040	18	21	30	37
T3	0.15	56/239	33/66	14	20	31	39
All tensors				39	49	59	66
Gilgit (110F) Dainyor Diorite							
T1	0.5	28/193	04/101	24	36	45	51
T2	0.8	78/124	11/277	16	25	34	51
All tensors				34	45	53	63
Hunza (85F) Southern Karakorum Metasediments							
T1	0.4	17/086	05/177	24	32	41	44
T2	0.18	07/085	82/250	21	32	40	44
T3	0.4	87/286	01/177	21	25	32	47
All tensors				44	55	64	71
Karakorum N (122F) Northern Karakorum Metasediments							
T1[d]	0.3	10/350	06/259	17	26	36	44
T2[d]	0.8	85/074	05/253	14	22	30	45
T3	0.1	12/344	68/107	18	25	30	37
All tensors				35	43	51	63
Nanga Parbat (182F) Nanga Parbat Core (High-Grade Gneiss and Migmatites)							
T1	0.75	64/115	06/217	21	29	39	48
T2	0.5	45/115	06/211	15	25	36	50

Table 3. (continued)

Tensor	Φ	σ1	σ3	α < 12° (%)	α < 20° (%)	α < 30° (%)	α < 45° (%)
T3	0.25	62/028	27/191	18	28	34	43
All tensors				47	61	69	76
			Randu (136F) Ladakh, Askor Amphibolites				
T1	0.66	74/075	12/212	14	22	32	40
T2	0.5	42/152	09/054	17	22	27	33
All tensors				30	41	51	63

[a]Axis orientations given as plunge/plunge direction. Percentage of faults for which the misfit angle between the observed and calculated striae is less than 12°, 20°, 30°, and 45°. For each area, the tot gives the percentage of fitting data when taking into account all the tensors (two to four tensors) for the given area.
[b]Mainly radial extension, two preferred orientations well defined by specific faults.
[c]T3 recalculated on a residue of 42 faults explained neither by T1 nor T2.
[d]Possible inversion of σ1 and σ2, but with each tensor well defined by specific faults.

stress fields show strong spatial variability at the map scale. This is especially evident from the σ3 orientations, which show clearly distinct patterns to the west and east of Nanga Parbat. The western limit of Nanga Parbat (i.e., the MMT reactivated by the Quaternary Raikhot fault) thus appears as a first-order tectonic contact, between two crustal blocks with a different tectonic history or mechanical behavior. To the east, in a zone including the Nanga Parbat anticline, but also the Deosai Plateau, the Indus valley north of it and the Dassu dome, averaged σ3 orientations are predominately oriented NNE–SSW to NNW–SSE, whereas to the west, in Kohistan and the western Karakorum, the orientation of σ3 is predominantly E–W. Third, most tensors indicate horizontal extension (i.e., are characterized by steeply dipping σ1), especially in the eastern block, while the region is in a convergent kinematic regime: Himalayan convergence has averaged 20 mm a^{-1} [e.g., *DeCelles et al.*, 2002; *Guillot et al.*, 2003] since Eocene collision up to the present-day, and up to 20 mm a^{-1} shortening is currently recorded in the central Himalaya [*Larson et al.*, 1999; *Paul et al.*, 2001; *Jouanne et al.*, 2004].

4.2. Site-to-Site Variation of the Paleostress Orientations

[34] For each site, we have processed the set of fault data following the same approach as above for the stations grouped per zone. To ensure more robust stress determinations, we have systematically test back the assumed tensors on the set of faults to determinate for each fault the misfit between the theoretical and observed striae orientation, and clearly individualize the faults fitting the tensor. In many stations, more than one tensor is required to explain the observed slip movements. Only the two best defined ones have been retained, the others being constrained by a too low number of faults. Because of the large number of data, only a few characteristic fault distribution patterns are given hereafter (Figure 9, localization of the sites, Figure 3), the results for all the stations being summarized in Table S1.

[35] Station 06-13 (Astor valley, eastern Nanga Parbat cover, Figure 9a) is an example of the most common pattern: no clear preferred orientation of the faults, slip best explained by at least two tensors, each tensor T1 and T2 being defined by a significant amount of specific faults, even if part of the observed striae can be explained equally well by both tensors. Figure 9a shows the faults compatible with T1 or T2 with misfits <30°: 10 faults are common to both tensor, 11 faults fit only with T1 and 8 only with T2; for a threshold of 12°, only 2 faults are common to both tensors, but there are still 10 and 7 faults compatible with T1 and T2, respectively. In this station, striae superposition on some faults indicates that T1-related slips probably occurred prior to T2-related slips.

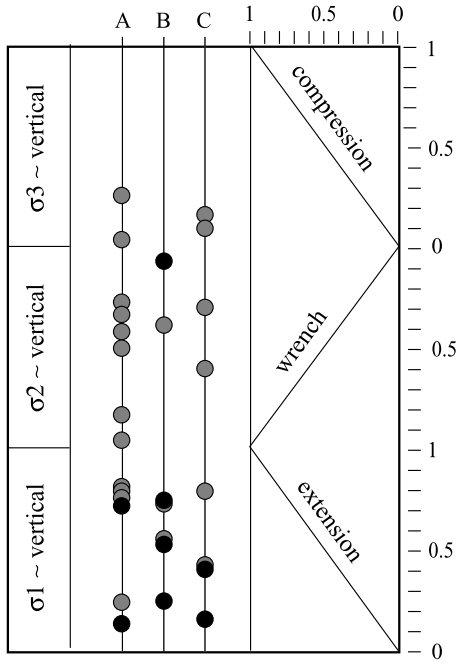

Figure 7. Grouped sites. Tectonic regime summary shows the strain regime. Horizontal and vertical scales indicate Φ ratio value (see text). Vertical lines are A for west of the Raikhot fault, in Kohistan (gray symbols) and Besham area (black symbols); B for east of the Raikhot fault, in Nanga Parbat (black symbols) and Ladakh; and C for north of the MKT, in Karakorum (black symbols: Braldu-Dassu area).

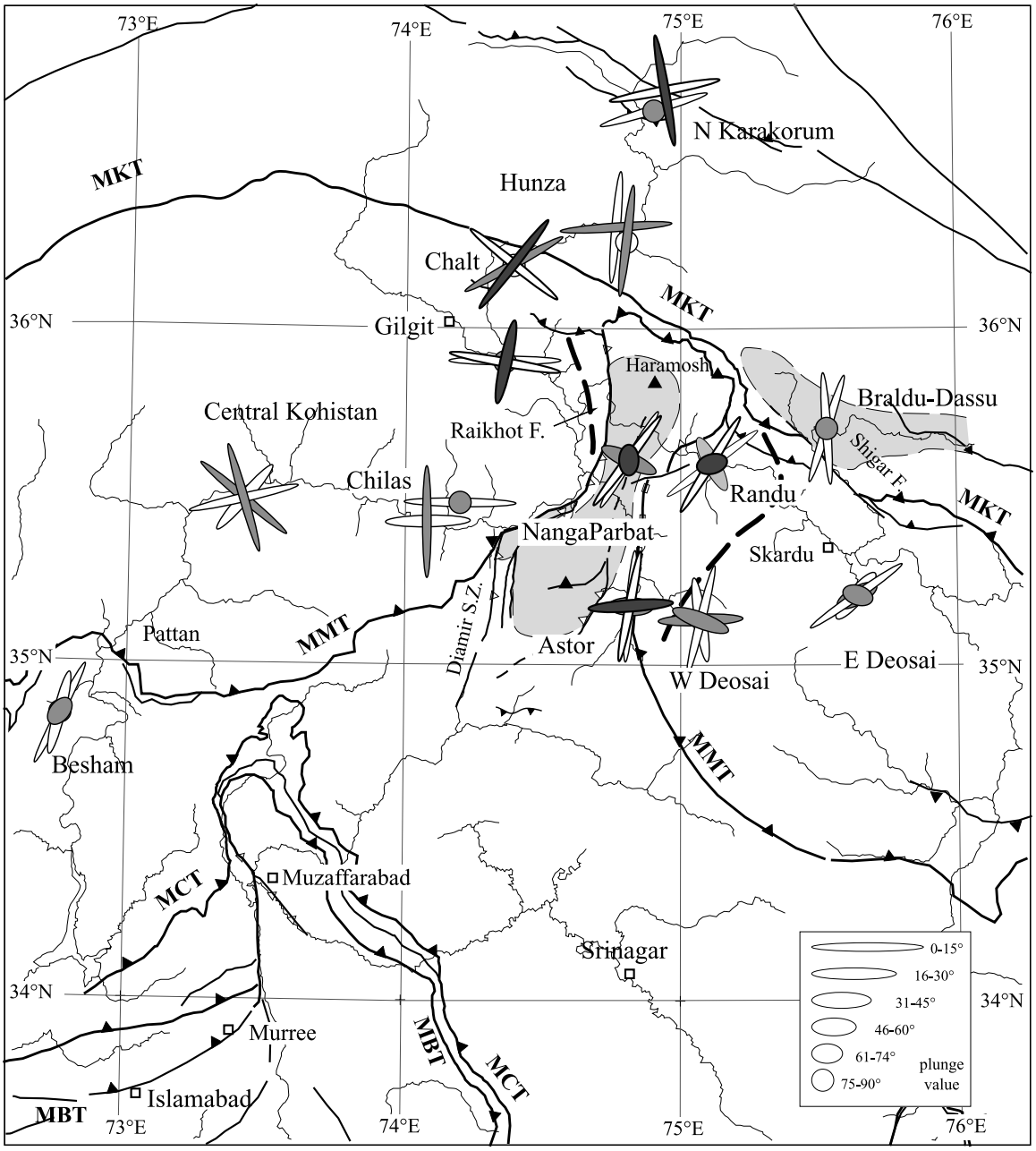

Figure 8. Regional stress orientations in northern Pakistan. Tensors are calculated by merging faults measured in 4 to 11 individual outcrop-scale sites (see Figure 3). Each stress axis is indicated by an ellipse: the great axis of the ellipse gives the azimuth of the principal stress axis, the shape of the ellipse its plunge (classes of 15°). For each area, only the two best tensors (see text and Table 3) are shown. For T1, $\sigma 1$ in black, $\sigma 3$ thick plain symbol; for T2, $\sigma 1$ in gray, $\sigma 3$ light plain symbol. Shaded area indicates zones of Plio-Quaternary very active exhumation; thick dashed line indicates eastern morphological limit of the Nanga Parbat area.

[36] Station 00-67 (Deosai plateau, Kohistan, Figure 9b) illustrates another frequent situation: despite the low number of measured faults, it seems possible to define two tensors T1 and T2. If we accept misfits of 30°, 3 faults are common to both tensors, 7 faults fit only with T1 and 7 only with T2; for a threshold of 12°, no faults are common to both tensors, but there are still 5 and 6 faults compatible with T1 and T2, respectively. In this station, faults compatible with T1 have chlorite-epidote coating, and are probably older than the "colder" faults corresponding to T2 that do not show such coating. This station thus provides evidence

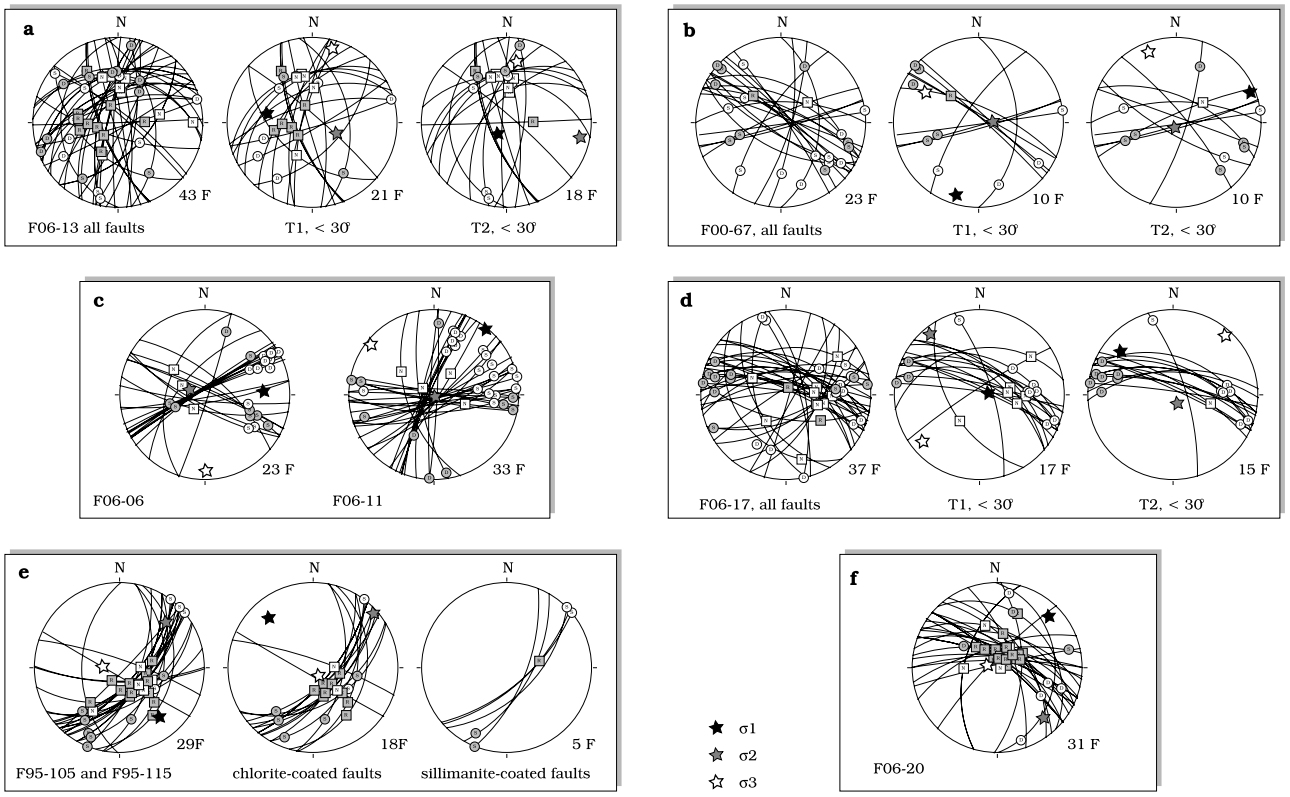

Figure 9. Fault/striae patterns from some typical sites. Stereographic projection, Wulff net lower hemisphere (same conventions as Figure 4). Localization of the sites is given Figure 3.

of an older NNE–SSW compression, which has not been evidenced in this area when grouping the stations in zones.

[37] The stations 06-06 and 06-11 (Hunza and Chalt area, respectively, Figure 9c) illustrate the simple case of two conjugate sets of strike-slip faults. In this case, a single tensor can account for most of the faults (74% and 82% of the faults, respectively, for a maximum misfit of 30°). The calculated tensor is in good agreement with the regional tensor calculated for both areas. Nevertheless, normal faults crosscutting strike-slip faults in these stations indicate here too the superposition of a second tensor with steeply plunging $\sigma 1$.

[38] Station 06-17 (Kohistan, Figure 9d) is a case where the stress tensor is poorly defined by one predominant set of faults. Two tensors can be defined, corresponding to a permutation of $\sigma 1$ and $\sigma 2$. If we consider misfits <30°, only 6 and 5 faults are specific to T1 and T2, respectively, and 11 faults can be explained indifferently by T1 and T2. Such a pattern suggests instability in the stress state or in the inversion. Striae superposition observed in the field, however, support two distinct episodes, with T1 preceding T2.

[39] Figure 9e does not correspond to a single station, but groups faults measured along the upper part of the Fairy Meadow road (Tato valley, stations 95-105 and 95-115), in high-grade migmatitic gneiss of the Nanga Parbat core, close to its western limit. In this area, we observe mylonitic structures striking predominantly NNE–SSW, i.e., parallel to the Nanga Parbat axis and to the Quaternary Raikhot fault. The oldest structures are left lateral shear zones with S-C type fabrics. As discussed by *Argles and Edwards* [2002], they predate Neogene Nanga Parbat anticline formation, as well as the high-temperature (sillimanite + cordierite anatexis) Neogene metamorphism observed in the core of the anticline. They probably trace southward thrusting of the Kohistan-Ladakh zone on top of the Himalayan gneisses. The S-C fabric is reactivated as sillimanite-coated strike-slip faults developed during or just after the peak of Neogene high-temperature metamorphism, and subsequently as chlorite coated reverse faults during the Pliocene-Quaternary temperature decrease (biotite Ar/Ar ages less than 5 Ma [*Schneider et al.*, 2001]). It is possible to calculate a tensor on the bulk set of fault, but this is meaningless given the clear temporal evolution observed in the field. It is more useful to consider the tensor calculated using only the chlorite coated reverse faults, which provides a single tensor T1, compatible with westward thrust component on the Raikhot fault, which corresponds to the last steps of the NNW–SSE Nanga Parbat shortening. The sillimanite-coated strike-slip faults correspond to another, older tensor, the orientation of which is undeterminable.

[40] Last, Figure 9f shows the faults of station 06-20, measured at the tip of the Murree syntaxis, just north of the MBT, in Lesser Himalaya metasediments. The stress tensor cannot be precisely fixed, but the $\sigma 1$ orientation (NNE–SSW to NE–SW) is clearly compatible with the

focal mechanism of the Balakot earthquake (Global CMT Catalog).

[41] Altogether, analyzing the data on a site per site basis reveals a complex and heterogeneous pattern. Most stations require more than one tensor to explain their set of measurements. The map in Figure 10 shows a simplified image of the results, as only the orientation of the tensor accounting for the largest number of faults has been reported for each site. Because of this choice, the map mixes asynchronous data: the fact that several sites in the same region show different stress orientations more probably reflects a different imprint of subsequent tensors in the considered sites, rather than a sharp lateral discontinuity in stress regime. Nevertheless, the map confirms and completes the larger-scale results shown Figure 8.

[42] The Nanga Parbat spur again shows up as a dominant boundary in the stress regime, as it does structurally and geomorphologically. In Nanga Parbat and the area immediately to the east, three different situations can predominate depending on the site: (1) extension parallel to the anticlinal axis of Nanga Parbat (σ1 vertical, σ3 S–N to SSW–NNE), (2) shortening perpendicular to the fold axis (σ1 WNW–ESE to W–E, σ3 SSW–NNE to S–N) and (3) in several sites, σ3 roughly parallel to the anticlinal axis but intermediate plunges of σ1. This variation is most easily explained by rotation of the fault sets, with a rotation axis parallel to the anticlinal axis. These features thus fit with a fold growing in a strain regime characterized by shortening parallel to the belt, as also suggested by the pattern of geochronological ages [*Schneider et al.*, 2001].

[43] We note that the zone displaying this pattern has a larger extension than the zone of unroofed Himalayan gneisses, i.e., the Nanga Parbat spur bounded by the MMT trace. To the east, it includes a strip of Ladakh Arc formations, of approximately the same width as the Nanga Parbat spur itself. The eastern limit of this strip is not well defined (Figure 10), but approximates the morphological limit of Nanga Parbat. It corresponds to the eastern end of the deep Indus gorge, which is characterized by high incision rates [*Burbank et al.*, 1996; *Leland et al.*, 1998], and to the eastern limit of the Astor river gorge, which is followed to the east by the Dassu-Deosai zone of much smoother relief. West of the Nanga Parbat spur, we find this characteristic stress pattern (SSW–NNE σ3, e.g., station 95-153, Table S1 in the auxiliary material) only in a narrow corridor of <2 km width west of the northern ending of the Sassi-Raikhot fault (i.e., the Quaternary reactivated MMT).

[44] Altogether, the stress pattern in and around Nanga Parbat is consistent with a large zone of vertical extrusion in an asymmetrical west vergent dome. The Himalayan middle crust currently extrudes in the western part of the dome, the Nanga Parbat anticlinorium itself. The structural asymmetry may correspond to a transient state in a system where the Nanga Parbat fold progressively widens to the east, but we have currently no evidence for such an evolution. Another possibility is that it is due to mechanical weakening by the extrusion of Himalayan gneiss on the western flank of the massif after the erosion of the hanging wall, and amplification of the fold by a feedback process between erosion, exhumation and rock uplift (as suggested by *Zeitler et al.* [2001a, 2001b]). Cooling ages indicate that ductile displacement on the reverse shear zones bordering the Nanga Parbat pop-up on both sides (i.e., the Diamir and Rupal shear zones) ceased before the onset of vertical ductile flow in the core of the massif (2.3 Ma versus 1 Ma [*Schneider et al.*, 2001]), supporting the hypothesis of progressive strain localization.

[45] Southward from Nanga Parbat, we do not have sufficient data to fix the limit between a Kohistan-type stress regime (as observed, for instance, in the Chilas area: roughly N–S σ1 and E–W σ3) and Nanga Parbat-type stress regime (steep or E–W σ1 and N–S σ3). Only one site is located directly south of the Nanga Parbat spur, in the Nangi Mali area [*Pêcher et al.*, 2002]. Here, ductile structures (thrusts and folds) strike parallel to the Himalayan trend (WNW–ESE), but we obtain a stress tensor with the same orientation as in the main Nanga Parbat structure, indicating shortening parallel to the belt.

[46] On both sides of the Nanga Parbat zone as defined above, in Ladakh–Deosai and Kohistan as well as in the Karakorum, wrench strain is predominant (σ1 and σ3 horizontal). It marks the bulk Himalayan convergence, with a σ1 orientation close to north–south (consistent with shortening more or less parallel to the convergence orientation) and a σ3 orientation close to east–west (indicating lateral extrusion perpendicular to the convergence orientation).

5. Discussion

[47] A major challenge to paleostress studies in multiple deformed areas is establishing an absolute or even a relative chronology of the stress events. Field observations can help to constrain this chronology, for instance, by considering fault intersection criteria, superposition of striae, or the mineralogical nature of the fault gouge. In the sites we studied in northern Pakistan, however, we found only few unambiguous field criteria to establish a relative chronology of the faults. Moreover, the relation between a set of faults and any particular tensor might be ambiguous, as the same fault/striae pair can be activated by more than one tensor. Absolute dating of the minerals crystallized on the fault plane or in the fault gouge could, in principle, constrain the age of the faults. In northern Pakistan, however, appropriate minerals are rare: most faults are dry (i.e., no minerals are developed on the fault plane, or minerals have been dissolved) or show mainly argilaceous products. Chlorite-calcite-epidote or chlorite-quartz assemblages are rare and micaceous coats even more so. In addition, we frequently observed indications for fluid circulation (mostly in the form of extension veins superimposed on striations or secondary crystallization), which contaminate any mineral that may correlate with fault displacement. Nevertheless, despite the difficulty of dating the events directly from individual fault observations, the timing of stress events and brittle deformation in northern Pakistan can be bracketed indirectly by the more easily dated ductile tectonics and by

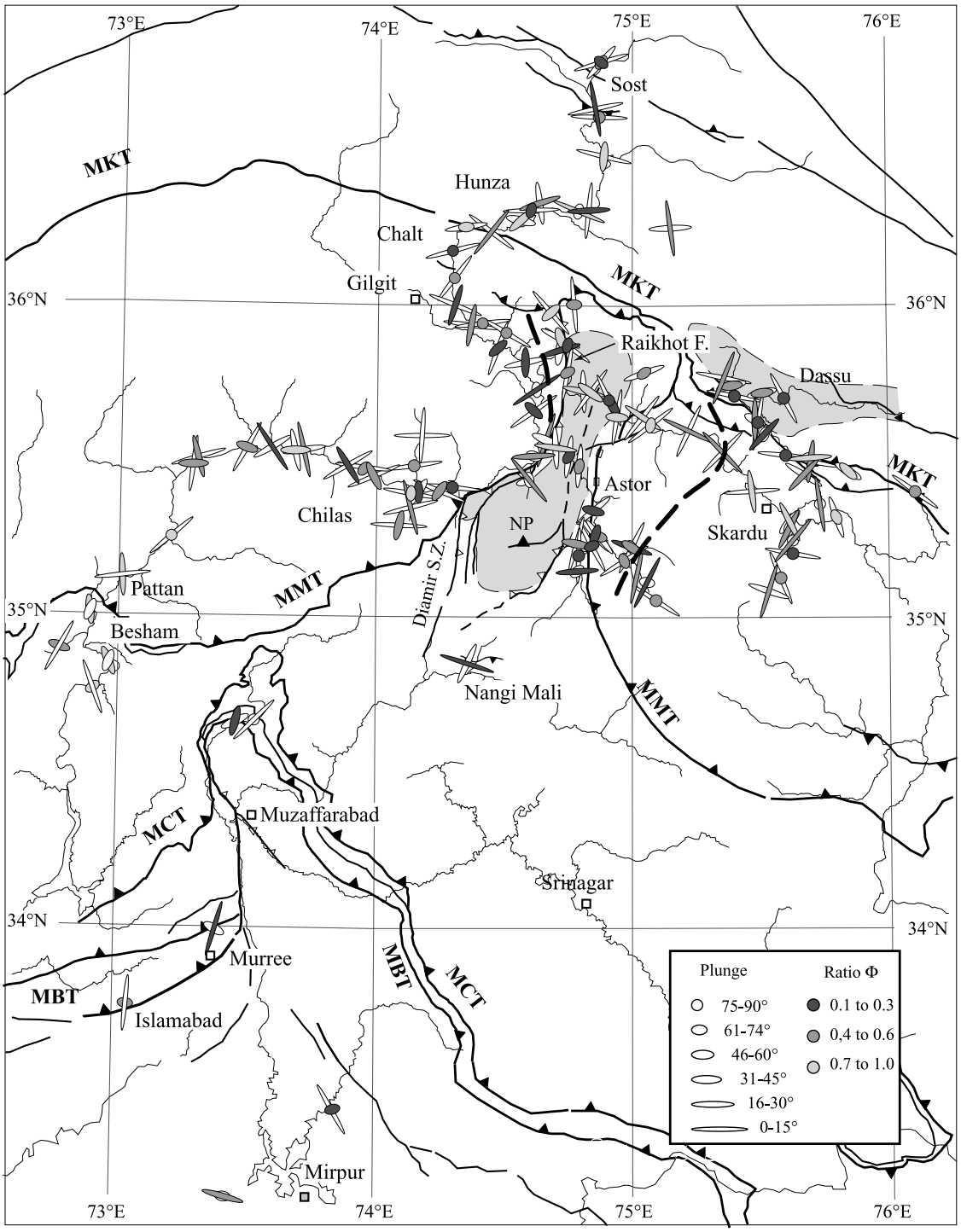

Figure 10. Paleostress orientations from individual site measurements. In each site, only the tensor with the largest number of fitting faults is plotted. Stress is represented by an ellipse, the great axis of which shows the principal stress axis orientation, whereas its ellipticity represents the plunge (from nearly horizontal, high ellipticity, to nearly vertical, circle). Shape ratio Φ (low, medium, high) is indicated by the color of the $\sigma 1$ ellipse; $\sigma 3$, plain ellipse. Thick dashed line indicates eastern morphological limit of the Nanga Parbat area (see text for discussion).

the ages of exhumation, as provided by thermochronological data.

[48] Concerning the two domains evidenced at a regional scale and separated by the Raikhot fault, the different observed stress patterns probably reflect two different stages of the tectonic activity, of different ages. East of the Raikhot fault, most of the Nanga Parbat pop-up anticline was in the ductile deformation field up to recently, as indicated by 4 to 11 Ma monazite U/Pb ages obtained on the high-grade migmatitic gneisses [*Smith et al.*, 1992], 1 to 5 Ma Ar/Ar cooling ages of biotite obtained in these gneisses [*Treloar et al.*, 2000; *Schneider et al.*, 2001], the intrusion of granites as young as 1 Ma [*Zeitler at al.*, 1993], and the shallow (5–6 km) present-day brittle-ductile transition as revealed by seismic investigations [*Meltzer et al.*, 2001]. Given the high (60°C km^{-1}) geothermal gradient in the upper crust of the western Himalaya [*Winslow et al.*, 1994] and rates of exhumation that reached 5–10 mm a^{-1} over the past 3 Ma [*Schneider et al.*, 1999], we expect rocks currently outcropping within the Nanga Parbat core to have passed the brittle-ductile transition less than a few million years ago. Thus, brittle extension in this area must reflect mainly the recent (late Pliocene and Quaternary) stress state. In the Dassu dome area, high-temperature metamorphism in the core of the dome took place at 6–7 Ma, from U/Pb ages on monazite [*Smith*, 1993], at temperatures $\geq$ 750°C [*Rolland et al.*, 2001], and it cooled by exhumation through the Ar-Ar closure temperature in biotite at ~5 Ma [*Searle et al.*, 1989]. Thus the N–S to NNE–SSW extensional stress observed in these areas cannot be older than Plio-Pleistocene, and is associated with the exhumation of Nanga Parbat and the Karakorum domes. The stress tensors evidenced here correspond to recent deformation stages, without tectonic inheritance from older (pre-Pliocene) phases.

[49] West of the Raikhot fault, most of Kohistan appears to be tectonically stable and characterized by low exhumation rates, as indicated by zircon fission track ages (closure temperature ~240°C [e.g., *Brandon et al.*, 1998]) ranging from 15 to ~50 Ma [*Zeitler*, 1985; *Zeilinger et al.*, 2007]. In this region, the stress field deduced from the brittle deformation features is dominated by N–S shortening in a wrench strain regime. This shortening orientation is coherent with the bulk India-Asia convergence orientation, but not with the current NE–SW belt-scale shortening, as indicated by the present-day seismicity. It does fit with south vergent stacking of the Karakorum and Himalayan units, where ductile synmetamorphic nappe emplacement ended around 16 Ma [*Fraser et al.*, 2001]. Thus, the tensor for Kohistan appears to correspond to the average regional stress field during the Miocene or earlier, rather than to Plio-Pleistocene deformation. It is oblique to the MKT, implying transpression on this structure and explaining the right-lateral strike-slip movement observed on it.

[50] In fact, multistage brittle deformation has been recorded in nearly all the sites, as indicated by the fact that more than one tensor is required to explain the set of striated fault planes. Figure 10 shows only the most clearly expressed tensor for each site (i.e., the tensor explaining the largest number of faults movements) and thus provides a distorted image of the paleostress pattern as it probably mixes asynchronous tensors. A clearer site-to-site comparison arises when plotting separately the tensors compatible either with shortening, wrench or extensional deformation (corresponding to the $\sigma 3$, $\sigma 2$, $\sigma 1$ axis, respectively, being vertical or nearly vertical). For this analysis, we retained for each site the tensor(s) for which the three main axes were less than 20° away from vertical or horizontal (corresponding to untilted or slightly tilted tensors).

5.1. Compressional Stress Fields

[51] Figure 11a shows the $\sigma 1$ orientation for all sites in which we determine a tensor with $\sigma 3$ close to vertical, and both $\sigma 1$ and $\sigma 2$ close to horizontal. For each site, only $\sigma 1$ has been plotted, the color of the ellipse corresponds to the Φ ratio (from $\Phi > 0$, compressional regime, to $\Phi = 0$, transition to wrench regime). Only few sites retain a record of compressional tectonics. Nevertheless, it is possible to recognize the superposition of two (or possibly three) main orientations:

[52] WNW–ESE compression, parallel to the belt, is recorded on both sides of Nanga Parbat in Kohistan and less clearly in Ladakh. This stress field is consistent with initiation of the Nanga Parbat transverse fold by doming during upper Miocene times [*Schneider et al.*, 2001] and its subsequent evolution as a pop-up structure. We have not been able to recognize this stress tensor in the Nanga Parbat or its boundaries itself. The reasons are that the Nanga Parbat core was still in the ductile field at this time, whereas faults that were created or activated by E–W compression within the outer sequence will have been rotated or reactivated during subsequent fold amplification.

[53] NNE–SSW to NE–SW compression, perpendicular to the local orientation of the Himalayan arc, is recorded mainly east of Nanga Parbat, in Ladakh. This is parallel to the mean present-day convergence orientation in this part of the belt, as indicated, for instance, by earthquake focal mechanisms. In the Kashmir syntaxis, where the density of our measurements is much lower than in the north, we find the same compressional stress field in the Miocene Murree sandstones, folded in NNW-SSE striking isoclinal folds (site 06-20, Figure 10). This orientation of the compressional stress axis is in good accordance with the focal mechanism of the 2005 Balakot earthquake that took place in this area. The same compression orientation has been recorded in the Pattan area (Besham syntaxis) by *Zeilinger et al.* [2000], who also correlate it to the most recent (Pleistocene) stress field. In this area as well, the inferred recent stress field is in good accordance with focal mechanisms of the 1974 Pattan earthquake as well as aftershocks of the 2005 Balakot earthquake. We have not found indications for this compression orientation in the central part of Ladakh and Kohistan, which appear to react currently as rigid blocks, with deformation mainly concentrated on their borders.

[54] Compressional stress with a N–S to NN E–SSW oriented $\sigma 1$ axis has been observed in some outcrops in the Skardu area. The same $\sigma 1$ orientation is widely observed in

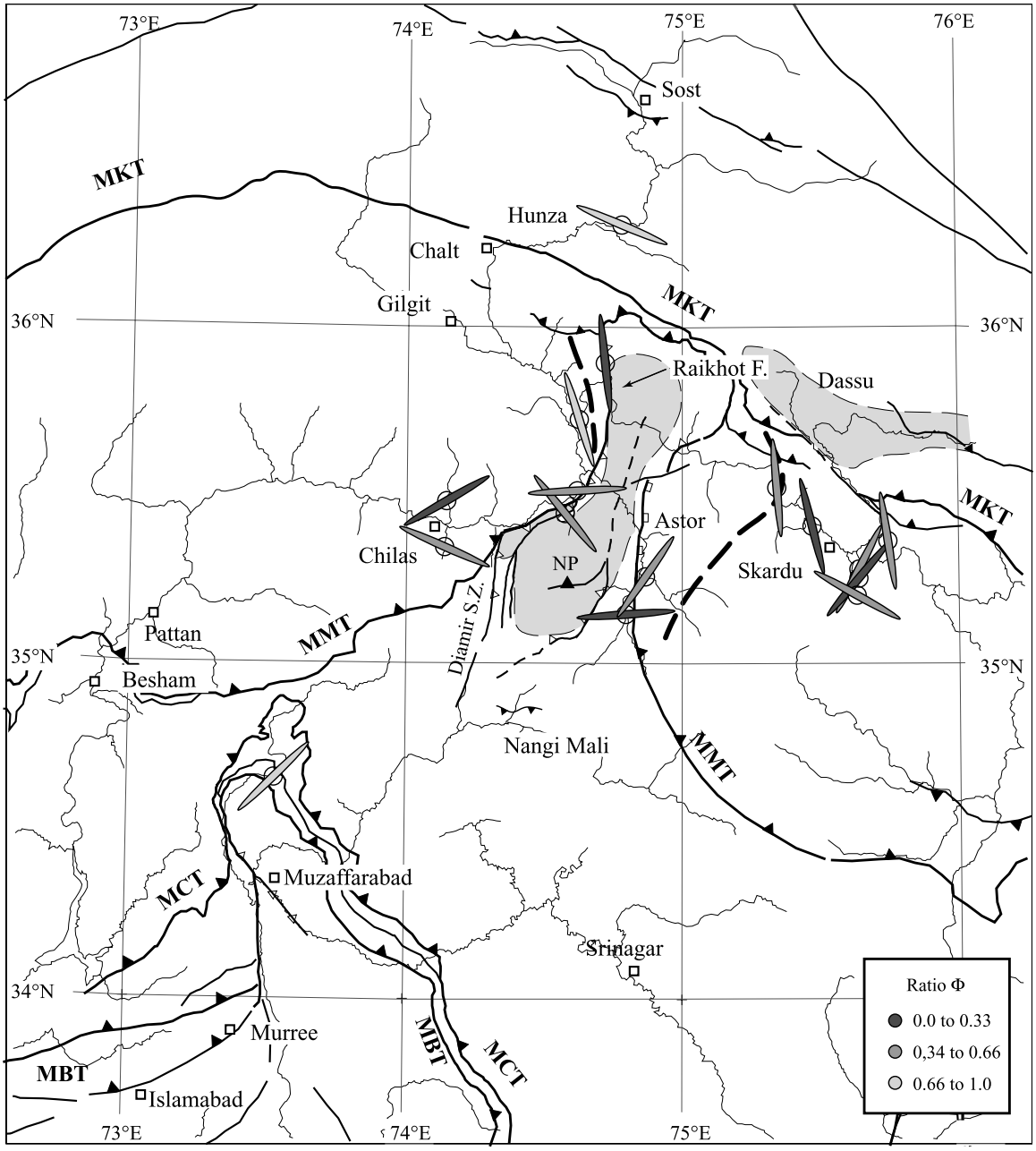

Figure 11a. Paleostress orientations from individual sites measurements. Compressional strain; $\sigma 3$ close to vertical (plunge >70°), $\sigma 1$ and $\sigma 2$ horizontal (plunge < 20°) Grey ellipses indicate orientation of $\sigma 1$.

Kohistan and Karakorum, but in a wrench tectonic context (see below). It is roughly parallel to the average Himalayan convergence orientation, but oblique with respect to modern convergence across the western Himalaya. The corresponding fault/striae couples could represent traces of brittle deformation dating from before the onset of Nanga Parbat exhumation (e.g., site 00-67, Figure 10, which feature a NNE–SSW compression prior to ENE–WSW compression), thus recording Miocene or older deformation.

5.2. Wrench-Type Stress Fields

[55] Figure 11b shows the $\sigma 1$ and $\sigma 3$ orientations for sites where both are close to horizontal. This situation corresponds to wrench-type strain, mainly marked by steeply dipping faults with low-pitch striae. We observe two of the main $\sigma 1$ orientations also observed in the compressional tensors; this parallelism suggests that the change from compression to wrenching corresponds to a permutation of the $\sigma 2$ and $\sigma 3$ axes in an unstable stress field.

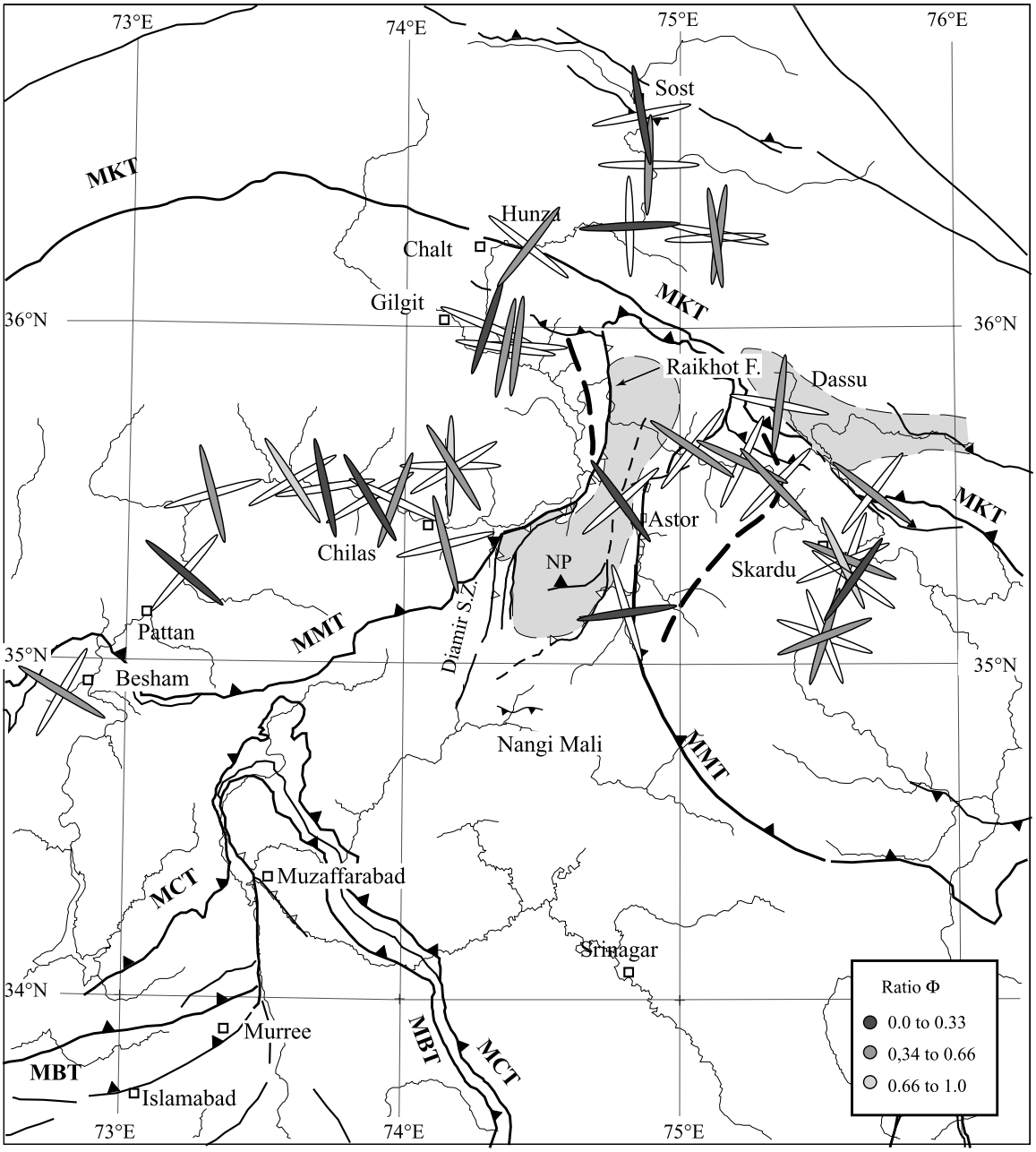

Figure 11b. Paleostress orientations from individual sites measurements. Wrench strain; $\sigma 2$ close to vertical (plunge >70°), $\sigma 1$ and $\sigma 3$ close to horizontal (plunge < 20°). Grey ellipses indicate orientation of $\sigma 1$. Plain ellipses: orientation of $\sigma 3$.

[56] Compression parallel to the belt is widely encountered east of the Raikhot fault, but not west of it, in the Kohistan block. This pattern suggests that deformation in the Kohistan block was inhibited, most of the shortening parallel to the belt being absorbed in the hot and ductile Nanga Parbat pop-up structure. It thus confirms the importance of the Raikhot fault as a major structural boundary between a rigid and cold Kohistan block to the west and a locally reheated Ladakh block to the east.

[57] The same stress orientation as east of the Nanga Parbat is observed in the Besham syntaxis, both in the hanging wall and footwall of the MMT. In this area, the tectonic pattern is similar to that encountered in Nanga Parbat: the MMT is folded in a large N–S anticline and the Himalayan series appear in the unroofed core of the syntaxis. The Besham syntaxis could be a second zone where shortening parallel to the belt is absorbed, but this zone has either been aborted, or is currently at a less

evolved stage than Nanga Parbat. In a previous study limited to this zone, *Zeilinger et al.* [2000] depicted the stress orientations using a direct inversion method (FSA code [*Célérier*, 1995]). They also found an E–W orientation for $\sigma 1$ and suggest, as we do, an early Pliocene age for this tensor, associated with the onset of Nanga Parbat extrusion. But instead of a wrench regime ($\sigma 2$ vertical), they found a compressional regime ($\sigma 3$ vertical); it is difficult to say if this discrepancy is due to different sampling of faults in the field, to the different processing of the data, or if it reflects some instability of the stress state. We favor the two last hypotheses, as both *Zeilinger et al.* [2000] and ourselves found tensors with low shape ratios Φ (close to 0). Such tensors are characterized by similar magnitudes for $\sigma 2$ and $\sigma 3$, allowing easy permutation from compression to wrench regimes. The difference may thus not be significant.

[58] Wrench-type stress fields with a N–S oriented $\sigma 1$ axis were found in central Kohistan and in the Karakorum. In northern Karakorum, our data are fully consistent with the previous data of *Zanchi and Gritti* [1996] in Sost area, acquired using the *Angelier* [1984] method. As previously discussed, stress tensors with N–S oriented $\sigma 1$ axis could correspond to a Miocene or earlier (pre-Nanga Parbat anticline) regional stress field. We have not found evidence for this stress tensor in the few sites that we have studied along the Indus in the Besham syntaxis. It has been found, however, by *Zeilinger et al.* [2000], who suggest a late Miocene to Pliocene age for it.

[59] The maps in Figures 10 and 11b suggest some reorientation of the stress field close to the MKT, in the Chalt-Gilgit area, where $\sigma 1$ appears to rotate to an orientation perpendicular to the MKT. Such rotation can be interpreted as a block boundary effect, that is, local rotation of the stress field against the Kohistan-Karakorum boundary, a zone of transpression, as indicated by dextral strike-slip displacement [*Coward et al.*, 1986]. It can also indicate different predominant imprints of late Miocene N–S shortening and modern NNE–SSW shortening perpendicular to the belt. Similarly, in central Kohistan the dominant $\sigma 1$ orientation is not N–S, but NNW–SSE. In this area, stress fields could have been partly controlled by the local orientation of the MKT to the NW and the MMT to the SE. However, our network of sites is not dense and wide enough to determine whether these variations are significant.

5.3. Extensional Stress Fields

[60] Figure 11c shows the sites for which a significant part of the fault set is accounted for by a tensor with $\sigma 1$ close to vertical (plunge > 70°). Such a stress field corresponds to extensional strain in the orientation of $\sigma 3$. The map underscores the widespread nature of extension, which is concentrated in the zones of recent ductile exhumation, but not restricted to those. The dominant $\sigma 3$ orientation is roughly W–E, i.e., slightly oblate to the belt (transtension), with not much change when moving from Karakorum to Kohistan, or from Kohistan to Ladakh. Similar extension is observed in the Nanga Parbat spur (Astor valley). This extension is marked by faults with chlorite coating or by dry faults, formed during cooling of the Nanga Parbat gneiss. Accordingly, it should be younger than 5 Ma, or even 2 Ma (average Ar/Ar mica ages in the core of this zone). If we assume that the W–E to WNW–ESE extension observed in Karakorum and from Gilgit to Skardu has the same age, it implies widespread post-5 Ma perpendicular to convergence extension in this part of the belt. However, we also recognize a N–S to NNW–SSE extension orientation in Nanga Parbat as well as in the Dassu area. As noted previously (compare Figure 9), this second orientation appears to be predominant east of the Raikhot fault, in the Nanga Parbat, Randu, and Braldu areas. Nevertheless, its pattern varies from site to site.

[61] In the central Nanga Parbat zone, ductile structures are dominated by NNE–SSW striking isoclinal folds, and a N–S stretching lineation, partly inherited from preceding MMT thrusting. Some N–S ductile extension, corresponding to normal-sense north oriented displacement, could have occurred in the footwall of the Main Mantle Thrust, prior to the Nanga Parbat fold formation [*Argles and Edwards*, 2002]. The N–S brittle extension observed in the same zone could mark the continuation of this extension from prior to 5 Ma (probable initiation of the Nanga Parbat fold) until at least 2 Ma. NNW–SSE to NNE–SSW extension is also observed in the Besham syntaxis [*Zeilinger et al.*, 2007], which we already argued to be a similar structure to Nanga Parbat, and where the deep gorge of the Indus River flowing down from central Kohistan may reflect recent uplift.

[62] North of Skardu, in the southern Karakorum, Pliocene exhumation of middle crust as in Nanga Parbat also occurs in the core of dome-shaped folds. We have measured fault sites only in the Dassu dome, the easternmost of a series of E–W trending domes between the right-lateral Shigar and Karakorum faults. If we consider the bulk set of faults from the four sites located on the Dassu dome (Braldu-Dassu area in Figure 8), the best defined tensors are characterized by vertical $\sigma 1$ and N–S oriented $\sigma 3$. In more detail, the multiple inverse method analysis for this area (Figure 12) shows a well-defined cluster for $\sigma 1$, implying that the vertical orientation obtained for $\sigma 1$ is robust. In contrast, $\sigma 3$ solutions are spread throughout the horizontal plane, with Φ ratios around 0.3 to 0.5. This pattern is characteristic of multidirectional extension, with only a weak preference for N–S extension, and thus mimics (and probably closely followed) ductile radial extension observed in the same domes [*Mahéo et al.*, 2004].

[63] At the northern termination of the Nanga Parbat anticline, the ductile gneissic fabric draws two juxtaposed domal structures, as indicated by the mapping of *Le Fort and Pêcher* [2002]. Fault sites located around the domes in this area also indicate radial extension, mimicking the earlier ductile extension marked by stretching lineations.

[64] The coexistence of N–S extension in both the Dassu dome and the Nanga Parbat and Besham syntaxes, which display different regional structural orientations (N–S for the Nanga Parbat and Besham syntaxis folds, E–W for the Karakorum domes), indicates that such extension was not only locally controlled by the geometry of the folds and

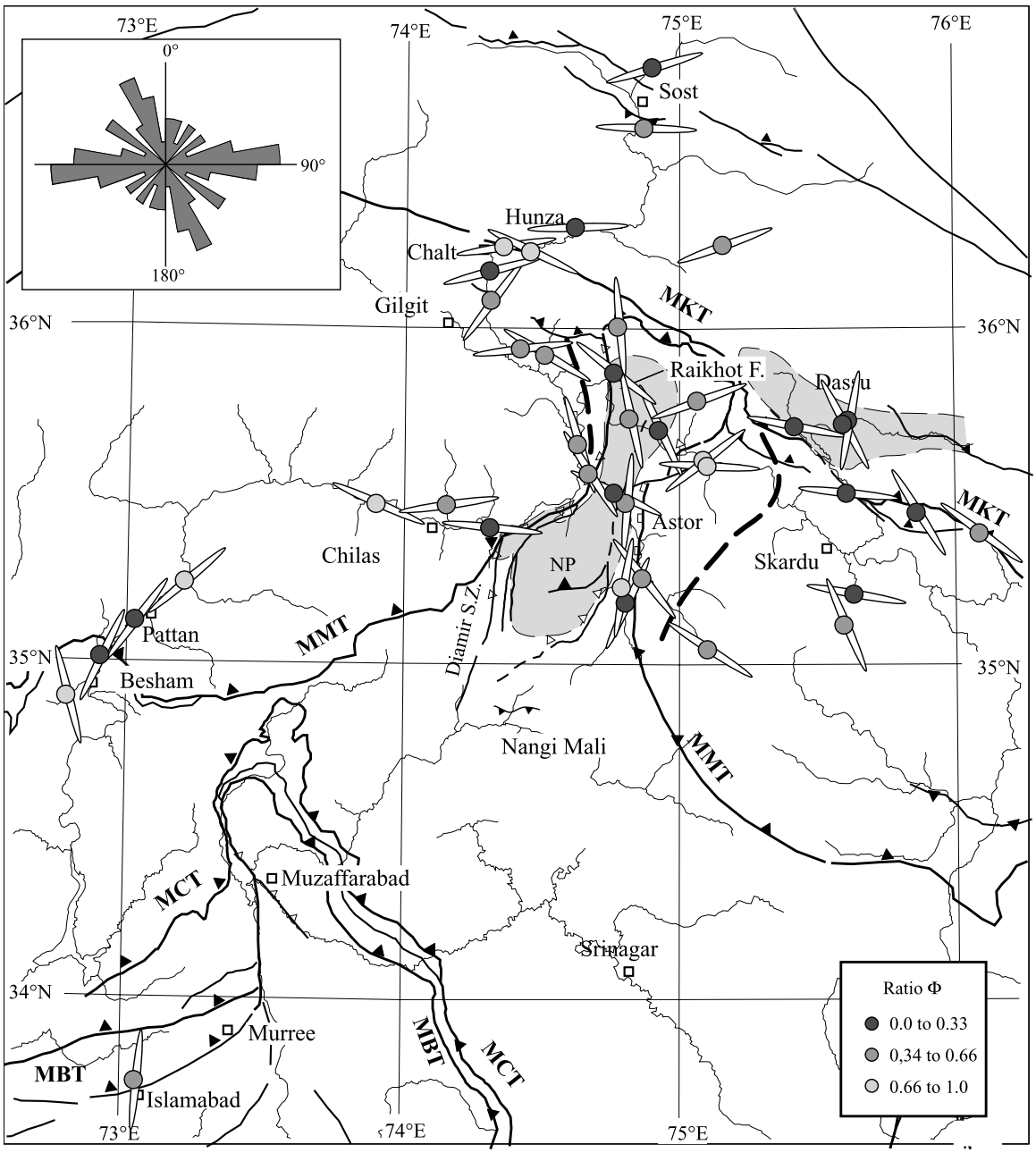

Figure 11c. Paleostress orientations from individual sites measurements. Extension strain; $\sigma 1$ close to vertical (plunge >70°), $\sigma 2$ and $\sigma 3$ horizontal (plunge < 20°) Plain ellipses indicate orientation of $\sigma 3$. The rose diagram shows the orientations of $\sigma 3$ (39 values, classes of 10°, maximum 6 values).

domes, but implies spreading of the crust at a larger scale (hundreds of kilometers). The same is true for E–W extension, which is observed in the Karakorum, northern Kohistan, and Ladakh. It is difficult to establish a relative chronology for these two regional Plio-Pleistocene extension orientations. Radial to N–S extension is common to both ductile and brittle regimes. We suggest that this brittle deformation is a continuation of the similarly oriented ductile deformation and would thus be older than WNW–ESE extension. This brittle extension is uncorrelated with the ductile strain pattern and may thus postdate Nanga Parbat doming. Actually, it corresponds to the present-day extension in this area, as indicated by the focal mechanism solutions.

5.4. Tilted Tensors

[65] Altogether, about one third of the calculated tensors have principal axes that are significantly tilted (more than

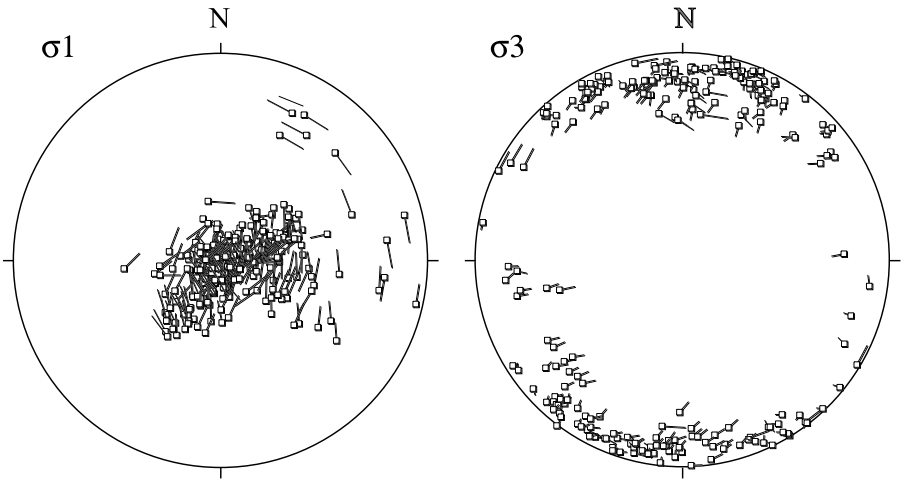

Figure 12. Dassu-Braldu area, results from the multiple inverse methods (software package mim5-miv4, A. Yamaji et al., Multiple Inverse Method Software Package, Freeware package, 2005, http://www.kueps.kyoto-u.ac.jp/~yamaji/PDS/indexe.html); 235 points (from a 60 000 nods grid) having a significant number of solutions tied to them [see *Yamaji et al.*, 2005], plotted in lower hemisphere, equal-area projections. (left) Stereogram for $\sigma 1$, clustered close to vertical. (right) Stereogram for $\sigma 3$, with a poorly defined NNE-SSW best position.

20°) with respect to the vertical or horizontal. These tensors are indicated on Figure 10 where the tilt of the principal axis is indicated by the degree of ellipticity of the symbol. They do not fit the widely accepted Andersonian faulting theory, which states that near the free surface, where shear stress is nil, one of the principal stress axes is normal to the surface and others two are parallel to it. In low-relief areas, these orientations are nearly vertical and horizontal, but in the high relief of the study region stress axes that obey Andersonian theory can be significantly oblique. The tilted tensors can thus be due to either local perturbations of the stress field by topography, or to passive postfaulting rotation of the set of faults on which the tensor was calculated.

[66] In northern Pakistan, the thermal gradient is particularly high in the rapidly exhuming areas (Nanga Parbat, eastern Karakorum), and lifts the brittle-ductile transition up to a few km below the surface. The brittle-ductile transition has been located from microseismicity at only 5–6 km depth below Nanga Parbat [*Meltzer et al.*, 2001] while topography over a distance of only 15 km ranges between 8 km at the summit of Nanga Parbat to 1 km along the Indus River. Topographic stresses can thus be expected to have a significant effect over the entire brittle crust.

[67] In effect, tilted tensors are mainly observed in the broad Nanga Parbat zone as previously defined (i.e., the Nanga Parbat spur and adjacent western Ladakh). The Nanga Parbat has evolved during the Pliocene as a pop-up anticline, extruded between two N–S ductile shear zones [*Schneider et al.*, 1999; *Edwards et al.*, 2000]: the Diamir shear zone, which is the southern prolongation of the Quaternary Raikhot fault to the west and the Rupal shear zone to the east (Figure 1). Recent exhumation of Nanga Parbat is concentrated in the core of the N–S anticline, at a rate of 5–10 mm a^{-1} [*Zeitler et al.*, 1993; *Schneider et al.*, 1999; *Zeitler et al.*, 2001a]. In many sites of this area, $\sigma 3$ remains roughly horizontal and parallel to the fold axis; $\sigma 1$ axis is not tilted around an axis parallel to the river gorges, as would be expected for topographic effects, but remains perpendicular to the fold, with various plunges (from horizontal to vertical). Thus in Nanga Parbat, tilted tensors can be most easily explained by passive rotation of the faults around the N–S axis of the growing pop-up anticline rather than by topographic effects.

6. Conclusions

[68] The aim of this study is to provide a comprehensive overview of the paleostress patterns in northern Pakistan. We have underlined the challenges associated with fault inversion studies in an area of multistage and heterogeneous deformation. The tasks include recognizing the superimposed tensors and establishing their chronology, using intrinsic information from the sites themselves.

[69] In a heterogeneous stress field, results could be sampling-dependent because the imprint of the different stress events is not the same at different sites. This could especially be a problem in zones of low-density sampling of faults. Results could also be partly method-dependent. For the southern part of our study area, we have been able to compare our results with those of two previous studies that employed a different inversion method [*Zeilinger et al.*, 2000; *Burg et al.*, 2005b]. At a regional scale, we obtained a similar superposition of stress regimes, i.e., successively NNE–SSW compression (in a compression or wrench strain regime), E–W compression, extension (E–W and radial instead of NW–SE), and finally NE–SW to NNE–

SSW compression (compatible with the Balakot earthquake). At a more local scale (for instance, along the Indus section in the Besham syntaxis), however, we notice some discrepancies such as different relative imprints of the successive tensors, slight orientation discrepancies, larger discrepancies in the Φ ratio and, associated with the latter, possible permutation of the $\sigma1-\sigma2$ or $\sigma2-\sigma3$ axes.

[70] The relative chronology and time bracketing of successive stress fields has been mainly based on regional continuity and comparison with better dated ductile tectonics. This proved a relatively easy task north of the MMT and in the Nanga Parbat area, where the density of measurement sites was sufficiently high to verify the coherence of the results from one site to another and to evidence regional trends. It was less successful in the Kashmir syntaxis to the south of Nanga Parbat where faults sites were scarcer, partly due to lack of propitious outcrops and partly due to access restrictions. Despite these limits, the applied method evidences a recent (mainly Pliocene and Pleistocene) paleostress pattern in northern Pakistan, which is well reflected by the main geomorphologic units.

[71] The oldest recorded stress field predates Pliocene-Quaternary exhumation of Nanga Parbat and Karakorum. It corresponds to NNE–SSW shortening in a wrench strain regime, in response to Indian-Asian convergence. The $\sigma1$ principal stress axis is roughly N–S, while $\sigma3$ is E–W. Its imprint is mainly preserved in Kohistan and Deosai, which were probably tectonically and morphologically stabilized as early as middle Miocene. It is also observed in the central Karakorum, however, which remained thermally active until at least the Upper Miocene, as indicated by emplacement of Sumayar leucogranite (Hunza area) at 9.2 Ma [*Fraser et al.*, 1999]. In the Karakorum, this initial stress field is coherent with the late nappe stacking to the south.

[72] The Mio-Pliocene initiation of the Nanga Parbat system of N–S trending folds marks the appearance of a new regional stress state, which also corresponds to wrenching, but with shortening oriented parallel to the belt ($\sigma1$ WNW–ESE, and $\sigma3$ SSW–NNE). The Nanga Parbat appears as a tectonic singularity, where most of the shortening is absorbed and the excess crustal volume eroded. Its western limit is the Raikhot fault: the imprint of the stress field characterized by E–W compression is clear to the east of this fault, in Ladakh and in the Nanga Parbat, but vanishes to the west of it. The Raikhot fault and its southward prolongation (the Diamir shear zone) act as a major N–S discontinuity, possibly inherited from a pre-Himalayan limit between two crustal segments of the crust with different bulk rheology within the Indian craton. The other main discontinuity is the vertical Shyok fault zone, which reactivates the Shyok suture zone and acts as a right-lateral transfer zone required to accommodate Nanga Parbat shortening. To the southwest of Nanga Parbat, the same paleostress orientation has been encountered in the Besham syntaxis, which could represent an aborted or immature structure similar to the Nanga Parbat pop-up.

[73] Plio-Pleistocene extension appears as an outstanding feature. It is predominantly multidirectional. Nevertheless, there seems to be a transition in time from a N–S to an E–W orientation of the main extension orientation. Strong exhumation of Nanga Parbat, lateral collapse of the hanging wall of the Nanga Parbat fold and final extrusion of the Dassu dome, are all associated with vertical $\sigma1$, and occurred during this extensional phase. This extension is not restricted to the zones of rapid exhumation, however, but appears widespread across northern Pakistan. This phase can possibly be linked to widespread E–W extension that affected the Tibetan Plateau farther east during the same period [*Armijo et al.*, 1986].

[74] Finally, we have observed NE–SW compression in Ladakh and in the northern part of the Kashmir syntaxis. This stress field is characterized by a $\sigma1$ axis perpendicular to the strike of the belt and parallel to present-day compression, as evidenced by earthquake focal mechanisms, in particular those of the 1974 Pattan and 2005 Balakot earthquakes.

[75] The timing of the first and last stages is best constrained. The relation between the stage(s) of compression parallel to the belt and the stage(s) of extension is more ambiguous. We propose a Mio-Pliocene age for shortening parallel to the belt, based on the age of the onset of N–S fold axis in Nanga Parbat. Along-strike compression is consistent with the *Seeber and Pêcher* [1998] model of strain partitioning along the Himalayan arc and the Nanga Parbat antiform. However, this model is based on the present-day geometry of the Himalayan arc and radial convergence, and we cannot be certain it applies for the Pliocene period. Moreover, the distribution of focused low-velocity anomalies below the Nanga Parbat inferred from geophysical data [*Zeitler et al.*, 2001a, and references therein] suggests rapid exhumation of rocks from midcrustal depths, which fits better with extension and a vertical $\sigma1$, as observed in the fault data and in seismicity (Figure 2), which indicates today ENE–WSW extension in Nanga Parbat.

[76] Regardless of the chronology at a million year scale of shortening parallel to the belt, extension parallel to the belt and vertical extrusion, the N–W Himalayan syntaxis is clearly a zone of tectonic and stress instability during its entire Pliocene-Quaternary history. Multidirectional extension is juxtaposed on short time periods to shortening either parallel or perpendicular to the belt. These differences may stem from stress axes permutations rather than changes in orientation. Such coexistence or juxtaposition could be typical of strain and stress partitioning during oblique convergence.

[77] **Acknowledgments.** This work summarizes data collected during many campaigns of field work in northern Pakistan and has benefited during the last years from the support of the Geological Survey of Pakistan, the French Embassy in Islamabad, and the ANR program PAKSIS. We thank two referees for their constructive and very detailed reviews.

References

Angelier, J. (1975), Sur l'analyse des mesures recueillies dans des sites faillés: L'utilité d'une confrontation entre les méthodes dynamiques et cinématiques, *C. R. Acad. Sci.*, *281*, 1805–1808.

Angelier, J. (1979), Determination of the mean principal directions of stresses for a given fault population, *Tectonophysics*, *56*, T17–T26, doi:10.1016/0040-1951(79)90081-7.

Angelier, J. (1984), Tectonic analysis of fault slip data sets, *J. Geophys. Res.*, *89*, 5835–5848, doi:10.1029/JB089iB07p05835.

Argles, T. W., and M. A. Edwards (2002), First evidence for high-grade, Himalayan-age synconvergent extension recognised within the western syntaxis—Nanga Parbat, Pakistan, *J. Struct. Geol.*, *24*, 1327–1344, doi:10.1016/S0191-8141(01)00136-5.

Armijo, R., E. Carey, and A. Cisternas (1982), The inverse problem in microtectonics and the separation of tectonic phases, *Tectonophysics*, *82*, 145–160, doi:10.1016/0040-1951(82)90092-0.

Armijo, R., P. Tapponnier, J. L. Mercier, and H. Tong-Li (1986), Quaternary extension in southern Tibet: Field observations and tectonic implications, *J. Geophys. Res.*, *91*, 13,803–13,872, doi:10.1029/JB091iB14p13803.

Armijo, R., P. Tapponnier, and H. Tonglin (1989), Late Cenozoic right-lateral strike-slip faulting in southern Tibet, *J. Geophys. Res.*, *94*, 2787–2838, doi:10.1029/JB094iB03p02787.

Avouac, J. P., and P. Tapponnier (1993), Kinematic model of active deformation in central Asia, *Geophys. Res. Lett.*, *20*(10), 895–898, doi:10.1029/93GL00128.

Bendick, R., and R. Bilham (2001), How perfect is the Himalayan arc?, *Geology*, *29*, 791–794, doi:10.1130/0091-7613(2001)029<0791:HPITHA>2.0.CO;2.

Bertrand, J., J. Kienast, and J. Pinardon (1988), Structure and metamorphism of the Karakorum gneisses in the Braldu-Baltoro valley (north Pakistan).), *Geodin. Acta*, *2*, 135–150.

Bishop, A. W. (1966), The strength of solids as engineering materials, *Geotechnique*, *16*, 91–130.

Bossart, P., and R. Ottiger (1989), Rocks of the Murree Formation in Northern Pakistan: Indicators of a descending foreland basin of late Palaeocene to middle Eocene age, *Eclogae Geol. Helv.*, *82*, 133–165.

Bott, M. H. P. (1959), The mechanics of oblique slip faulting, *Geol. Mag.*, *96*, 109–117.

Brandon, M. T., M. Roden-Tice, and J. I. Garver (1998), Late Cenozoic exhumation of the Cascadia accretionary wedge in the Olympic Mountains, northwest Washington State, *Geol. Soc. Am. Bull.*, *110*, 985–1009, doi:10.1130/0016-7606(1998)110<0985:LCEOTC>2.3.CO;2.

Burbank, D. W., R. G. H. Raynolds, and G. H. Johnson (1986), Late Cenozoic tectonics and sedimentation in the north-western Himalayan foredeep: II. Eastern limb of the northwest syntaxis and regional synthesis, *Spec. Publ. Int. Assoc. Sedimentol.*, *8*, 293–306.

Burbank, D. W., J. Leland, E. Fielding, R. S. Anderson, N. Brozovic, M. R. Reid, and C. Duncan (1996), Bedrock incision, rock uplift and threshold hillslopes in the northwestern Himalayas, *Nature*, *379*, 505–510, doi:10.1038/379505a0.

Burg, J. P., P. Nievergelt, F. Oberli, D. Seward, P. Davy, J. C. Maurin, Z. Diao, and M. Meier (1998), The Namche Barwa syntaxis: Evidence for exhumation related to compressional crustal folding, *J. Asian Earth Sci.*, *16*(2–3), 239–252, doi:10.1016/S0743-9547(98)00002-6.

Burg, J. P., L. Arbaret, N. M. Chaudhry, H. Dawood, S. Hussain, and G. Zeilinger (2005a), Shear strain localization from the upper mantle to the middle crust of the Kohistan Arc (Pakistan), in *Fluid Motions in Volcanic Conduits: A Source of Seismic and Acoustic Signals*, edited by S. J. Lane and J. S. Gilbert, *Geol. Soc. Spec. Publ.*, *245*, 25–38, doi:10.1144/GSL.SP.2005.245.01.02.

Burg, J. P., B. Célérier, N. M. Chaudhry, M. Ghazanfar, F. Gnehm, and M. Schnellmann (2005b), Fault analysis and paleostress evolution in large strain regions: Methodological and geological discussion of the southeastern Himalayan fold-and-thrust belt in Pakistan, *J. Asian Earth Sci.*, *24*, 445–467, doi:10.1016/j.jseaes.2003.12.008.

Butler, R. W. H., and D. J. Prior (1988), Tectonic controls on the uplift of the Nanga Parbat Massif, Pakistan Himalayas, *Nature*, *333*, 247–250, doi:10.1038/333247a0.

Célérier, B. (1995), Tectonic regime and slip orientation of reactivated faults, *Geophys. J. Int.*, *121*, 143–161, doi:10.1111/j.1365-246X.1995.tb03517.x.

Coward, M. P., D. C. Rex, M. Asif Khan, B. F. Windley, R. D. Broughton, I. W. Luff, M. G. Petterson, and C. J. Pudsey (1986), Collision tectonics in the NW Himalayas, in *Collision Tectonics*, edited by M. P. Coward and A. C. Reis, *Geol. Soc. Spec. Publ.*, *19*, 203–219.

Coward, M. P., R. W. H. Butler, M. Asif Khan, and R. J. Knipe (1987), The tectonic history of Kohistan and its implication for Himalayan structure, *J. Geol. Soc.*, *144*(3), 377–391, doi:10.1144/gsjgs.144.3.0377.

DeCelles, P. G., D. M. Robinson, and G. Zandt (2002), Implications of shortening in the Himalayan fold-thrust belt for uplift of the Tibetan Plateau, *Tectonics*, *21*(6), 1062, doi:10.1029/2001TC001322.

DiPietro, J. A., and K. R. Pogue (2004), Tectonostratigraphic subdivisions of the Himalaya: A view from the west, *Tectonics*, *23*, TC5001, doi:10.1029/2003TC001554.

DiPietro, J. A., A. Hussain, I. Ahmad, and M. A. Khan (2000), The main mantle thrust in Pakistan: Its character and extent, in *Tectonics of the Nanga Parbat Syntaxis and the Western Himalaya*, edited by M. A. Khan et al., *Geol. Soc. Spec. Publ.*, *170*, 375–393.

Edwards, M. A., W. S. Kidd, M. A. Khan, and D. A. Schneider (2000), Tectonics of the SW margin of the Nanga Parbat-Haramosh massif, in *Tectonics of the Nanga Parbat Syntaxis and the Western Himalaya*, edited by M. A. Khan et al., *Geol. Soc. Spec. Publ.*, *170*, 77–100.

Etchecopar, A., G. Vasseur, and M. Daignières (1981), An inverse problem in microtectonics for the determination of stress tensors from fault striation analysis, *J. Struct. Geol.*, *3*, 51–65, doi:10.1016/0191-8141(81)90056-0.

Fontan, D., M. Schouppe, C. J. Hunziker, G. Martinotti, and J. Verpkaeren (2000), Metamorphic evolution, ^{40}Ar-^{39}Ar chronology and tectonic model for the Neelum valley, Azad Kashmir, NE Pakistan, in *Tectonics of the Nanga Parbat Syntaxis and the Western Himalaya*, edited by A. Khan et al., *Geol. Soc. Spec. Publ.*, *170*, 431–453.

Fraser, J. E., M. P. Searle, R. R. Parrish, and S. R. Noble (1999), U-Pb geochronology on the timing of metamorphism and magmatism in the Hunza Karakorum (abstract), *Terra Nostra*, *99*(2), 45–46.

Fraser, J. E., M. P. Searle, R. R. Parrish, and S. R. Noble (2001), Chronology of deformation, metamorphism and magmatism in southern Karakoram Mountains, *Geol. Soc. Am. Bull.*, *113*, 1443–1455, doi:10.1130/0016-7606(2001)113<1443:CODMAM>2.0.CO;2.

Gaetani, M. (1997), The Karakorum Block in central Asia, from Ordovician to Cretaceous, *Sediment. Geol.*, *109*, 339–359, doi:10.1016/S0037-0738(96)00068-1.

Greco, A. (1991), Tectonics and metamorphism in the western Himalayan syntaxis area (Azad Kashmir, NE-Pakistan), *Mitt. Geol. Inst. Zurich*, *274*, 193 pp.

Greco, A., G. Martinotti, K. Papritz, J. G. Ramsay, and R. Rey (1989), The crystalline rocks of the Kaghan valley (NE-Pakistan), *Eclogae Geol. Helv.*, *82*(2), 629–653.

Grove, M., and T. M. Harrison (1996), ^{40}Ar diffusion in Fe-rich biotite, *Am. Mineral.*, *81*, 940–951.

Guillot, S., G. Garzanti, D. Baratoux, D. Marquer, G. Maheo, and J. de Sigoyer (2003), Reconstructing the total shortening history of the NW Himalaya, *Geochem. Geophys. Geosyst.*, *4*(7), 1064, doi:10.1029/2002GC000484.

Harrison, T. M., I. Duncan, and I. McDougall (1985), Diffusion of ^{40}Ar in biotite: Temperature, pressure, and compositional effects. (1985), *Geochim. Cosmochim. Acta*, *49*(11), 2461–2468, doi:10.1016/0016-7037(85)90246-7.

Jouanne, F., J. L. Mugnier, J. F. Gamond, P. Le Fort, M. R. Pandey, L. Bollinger, M. Flouzat, and J. P. Avouac (2004), Current shortening across the Himalayas of Nepal, *Geophys. J. Int.*, *157*, 1–14, doi:10.1111/j.1365-246X.2004.02180.x.

Kasmi, A. H., and Q. Jan (1997), *Geology and Tectonics of Pakistan*, 554 pp., Graphic Publ., Karachi, Pakistan.

Krol, M. A., P. K. Zeitler, G. Poupeau, and A. Pecher (1996), Temporal variations in the cooling and denudation history of the Hunza plutonic complex, Karakoram Batholith, revealed by ^{40}Ar/^{39}Ar thermochronology, *Tectonics*, *15*(2), 403–415, doi:10.1029/95TC02424.

Larson, K. M., R. Bürgmann, R. Bilham, and J. T. Freymueller (1999), Kinematics of the India-Eurasia collision zone from GPS measurements, *J. Geophys. Res.*, *104*, 1077–1093, doi:10.1029/1998JB900043.

Le Fort, P., and A. Pêcher (2002), An introduction to the geological map of the area between Hunza and Baltistan, Karakoram-Kohistan-Ladakh-Himalaya region, northern Pakistan, scale 1:150,000, *Geologica*, *6*, 1–199.

Leland, J., M. R. Reid, D. Burbank, R. Finkel, and M. Caffee (1998), Incision and differential bedrock uplift along the Indus River near Nanga Parbat, Pakistan Himalaya, from ^{10}Be and ^{26}Al exposure age dating of bedrock straths, *Earth Planet. Sci. Lett.*, *154*, 93–107, doi:10.1016/S0012-821X(97)00171-4.

Liesa, C., and R. J. Lisle (2004), Reliability of methods to separate stress tensors from heterogeneous fault-slip data, *J. Struct. Geol.*, *26*, 559–572, doi:10.1016/j.jsg.2003.08.010.

Lode, W. (1925), Versuche über den Einfluss der mittleren Hauptspannung auf die Fliessgrenze, *Z. Angew. Math. Mech.*, *5*, 142–144.

Lombardo, B., and F. Rolfo (2000), Two contrasting eclogite types in the Himalayas: Implications for the Himalayan orogeny, *J. Geodyn.*, *30*, 37–60, doi:10.1016/S0264-3707(99)00026-5.

MacDougall, I., and T. M. Harrison (1999), *Geochronology and Thermochronology by the ^{40}Ar/^{39}Ar Method*, 2nd ed., 269 pp., Oxford Univ. Press, New York.

Mahéo, G., A. Pêcher, S. Guillot, Y. Rolland, and C. Delacourt (2004), Exhumation of Neogene gneiss domes between oblique crustal boundaries in south Karakorum (northwest Himalaya, Pakistan), in *Gneiss Domes in Orogeny*, edited by D. L. Whitney, C. Teyssier, and C. S. Siddoway, *Spec. Pap. Geol. Soc. Am.*, *380*, 141–154.

Meltzer, A., G. Sarker, B. Beaudoin, L. Seeber, and J. Armbruster (2001), Seismic characterization of an active metamorphic massif, Nanga Parbat, Pakistan, *Himalayan Geol.*, *29*, 651–654, doi:10.1130/0091-7613(2001)029<0651:SCOAAM>2.0.CO;2.

Nemcok, M., and R. J. Lisle (1995), A stress inversion procedure for polyphase fault/slip data sets, *J. Struct. Geol.*, *17*(10), 1445–1453, doi:10.1016/0191-8141(95)00040-K.

Otsubo, M., K. Sato, and A. Yamaji (2006), Computerized identification of stress tensor determined from heterogeneous fault-slip data by combining the multiple inverse method and k-means clustering, *J. Struct. Geol.*, *28*, 991–997, doi:10.1016/j.jsg.2006.03.008.

Parrish, R. P., and R. Tirrul (1989), U-Pb ages of the Baltoro granite, northwest Himalaya, and implica-

tions for monazite U-Pb systematics, *Geology*, *17*, 1076–1079, doi:10.1130/0091-7613(1989)017<1076:UPAOTB>2.3.CO;2.

Paul, J., et al. (2001), The motion and active deformation of India, *Geophys. Res. Lett.*, *28*, 647–650, doi:10.1029/2000GL011832.

Pêcher, A., and P. Le Fort (1999), Late Miocene tectonic evolution of the Karakorum-Nanga Parbat contact zone (northern Pakistan), in *Himalaya and Tibet: Mountain Roots to Mountain Tops*, edited by A. MacFarlane, J. Quade, and R. Sorkhabi, *Spec. Pap. Geol. Soc. Am.*, *328*, 145–158.

Pêcher, A., and L. Seeber (2003), Recent stress field in Nanga Parbat and southern Karakorum from faults inversion, paper presented at the 18th Himalaya-Karakoram-Tibet Workshop, ETH-Zurich, Ascona, Switzerland.

Pêcher, A., G. Giuliani, A. B. Kausar, R. M. Malik, and H. R. Muntaz (2002), Geology and geochemistry of the Nangimali ruby deposit area, Nanga-Parbat Himalaya (Azra Kashmir, Pakistan), *J. Asian Earth Sci.*, *21*(3), 265–282, doi:10.1016/S1367-9120(02)00041-X.

Poupeau, G., A. Pêcher, M. Benharbit, and O. F. Noyan (1991), Ages traces de fission sur apatites et taux de dénudation Plio-Quaternaires au Karakorum central, *C. R. Acad. Sci.*, *313*, 917–922.

Reuber, I. (1989), The Dras arc: Two successive volcanic events on eroded oceanic crust, *Tectonophysics*, *161*, 93–106, doi:10.1016/0040-1951(89)90305-3.

Robertson, A. H. F., and A. S. Collins (2002), Shyok Suture Zone, N Pakistan: Late Mesozoic-Tertiary evolution of a critical suture separating the oceanic Ladakh Arc from the Asian continental margin, *J. Asian Earth Sci.*, *20*, 309–351, doi:10.1016/S1367-9120(01)00041-4.

Rolland, Y., A. Pêcher, and C. Picard (2000), Middle Cretaceous back-arc formation and arc evolution along the Asian margin: The Shyook Suture Zone in northern Ladakh (NW Himalaya), *Tectonophysics*, *325*, 145–173, doi:10.1016/S0040-1951(00)00135-9.

Rolland, Y., G. Mahéo, S. Guillot, and A. Pêcher (2001), Tectono-metamorphic evolution of the Karakoram Metamorphic Complex (Dassu-Askole area, NE Pakistan): Mid-crustal granulite exhumation in a compressive context, *J. Metamorph. Geol.*, *19*, 717–737.

Rolland, Y., C. Picard, A. Pêcher, E. Carrio, S. M. F. Sheppard, S. M. Oddone, and I. Villa (2002), Presence and geodynamic significance of Cambro-Ordovician series of SE Karakoram (N Pakistan), *Geodin. Acta*, *15*, 1–21, doi:10.1016/S0985-3111(01)01075-0.

Rolland, Y., E. Carrio-Schaffhauser, S. M. F. Sheppard, A. Pêcher, and L. Esclauze (2006), Metamorphic zoning and geodynamic evolution of an inverted crustal section (Karakorum margin, N Pakistan), evidence for two metamorphic events, *Int. J. Earth Sci.*, *95*, 288–305, doi:10.1007/s00531-005-0026-x.

Schneider, D. A., M. A. Edwards, W. S. F. Kidd, M. Asif Khan, L. Seeber, and P. K. Zeitler (1999), Tectonics of Nanga Parbat, western Himalaya: Synkinematic plutonism within the doubly vergent shear zones of a crustal-scale pop-up structure, *Geology*, *27*, 999–1002, doi:10.1130/0091-7613(1999)027<0999:TONPWH>2.3.CO;2.

Schneider, D. A., P. K. Zeitler, W. S. F. Kidd, and M. A. Edwards (2001), Geochronologic constraints on the tectonic evolution and exhumation of Nanga Parbat, western Himalaya syntaxis, revisited, *J. Geol.*, *109*, 563–583, doi:10.1086/322764.

Scholz, C. H. (1988), The brittle-plastic transition and the depth of seismic faulting, *Geol. Rundsch.*, *77*, 319–328, doi:10.1007/BF01848693.

Scholz, C. H. (2002), *The Mechanics of Earthquakes and Faulting*, Cambridge Univ. Press, Cambridge, U.K.

Searle, M. P., A. J. Rex, R. Tirrul, D. C. Rex, A. Barnicoat, and B. F. Windley (1989), Metamorphic, magmatic and tectonic evolution of the Central Karakoram in the Biafo-Baltoro-Hushe regions of northern Pakistan, in *Tectonics of the Western Himalayas*, edited by L. L. Malinconico, *Spec. Pap. Geol. Soc. Am.*, *232*, 47–73.

Searle, M. P., M. A. Khan, J. E. Fraser, S. J. Gough, and M. Q. Jan (1999), The tectonic evolution of the Kohistan-Karakoram collision belt along the Karakoram Highway transect, north Pakistan, *Tectonics*, *18*(6), 929–949, doi:10.1029/1999TC900042.

Seeber, L., and A. Pêcher (1998), Strain partitioning along the Himalayan arc and the Nanga Parbat antiform, *Geology*, *26*, 791–794, doi:10.1130/0091-7613(1998)026<0791:SPATHA>2.3.CO;2.

Sharma, K. K., and K. R. Gupta (1978), Some observations on the geology of the Indus and Shyok valleys between Leh and Panamik, District of Ladakh, Jammu and Kashmir, India, *Recent Res. Geol.*, *7*, 133–143.

Smith, H. A. (1993), Characterization and timing of metamorphism within the Indo-Asian suture zone, Himalayas, northern Pakistan, Ph.D. thesis, Dartmouth Coll., Hanover, N. H.

Smith, H. A., C. P. Chamberlain, and P. K. Zeitler (1992), Documentation of Neogene regional metamorphism in the Himalayas of Pakistan using U-Pb in monazite, *Earth Planet. Sci. Lett.*, *113*, 93–105, doi:10.1016/0012-821X(92)90213-F.

Steck, A. (2003), Geology of the NW Indian Himalaya, *Eclogae Geol. Helv.*, *96*(2), 147–196.

Tahirkheli, R. A. K. (1982), Geology of the Himalaya, Karakorum, and Hindu Kush in Pakistan, *Geol. Bull. 15*, 51 pp., Univ. of Peshawar, Peshawar, Pakistan.

Tahirkheli, R. A. K. (1996), Map of tectonostratigraphic domains of Northern Collisional belts in Pakistan, scale 1:750000, MinRock Found., Geosci. Lab., Geol. Surv. of Pakistan, Islamabad.

Tahirkheli, R. A. K., M. Mattauer, F. Proust, and P. Tapponnier (1979), The India-Eurasia suture zone in northern Pakistan: Synthesis and interpretation of recent data of plate scale, in *Geodynamic of Pakistan*, edited by A. Farah and de K. A. S. Jong, pp. 125–130, Geol. Surv. of Pakistan, Quetta.

Treloar, P. J., et al. (2000), Geochronological constraints on the evolution of the Nanga parbat syntaxis, Pakistan Himalaya, in *Tectonic of the Nanga Parbat Syntaxis and the Western Himalaya*, edited by M. A. Khan et al., *Geol. Soc. Spec. Publ.*, *170*, 137–162.

Valdiya, K. S. (1998), *Dynamic Himalaya*, 178 pp., Univ. Press, Hyderabad.

Valli, F., N. Arnaud, P. H. Leloup, E. R. Sobel, G. Mahéo, R. Lacassin, S. Guillot, H. Li, P. Tapponnier, and Z. Xu (2007), Twenty million years of continuous deformation along the Karakorum fault, western Tibet: A thermochronological analysis, *Tectonics*, *26*, TC4004, doi:10.1029/2005TC001913.

Van Melle, J., P. A. van der Beek, S. Guillot, A. Pêcher, and M. Latif (2007), Slow steady exhumation of the high elevation Deosai Plateau (northern Pakistan Himalaya) since 40 Ma, *Eos Trans. AGU*, *88*(52), Fall Meet. Suppl., Abstract T20-7345.

Viganò, A., and S. Martin (2007), Thermorheological model for the European central Alps: Brittle-ductile transition and lithospheric strength, *Terra Nova*, *19*, 309–316, doi:10.1111/j.1365-3121.2007.00751.x.

Villa, I. M., Y. Lemennicier, and P. Le Fort (1996), Late Miocene to early Pliocene tectonometamorphism in south-central Karakorum and Indus-Tsangpo suture, Chogo Lungma area (NE Pakistan).), *Tectonophysics*, *260*, 201–214, doi:10.1016/0040-1951(96)00086-8.

Wadia, D. N. (1975), *Geology of India*, 4th ed., 508 pp., Tata McGraw-Hill, New Dehli.

Winslow, D. M., P. K. Zeitler, C. P. Chamberlain, and L. S. Hollister (1994), Direct evidence for a steep geotherm under conditions of rapid denudation, western Himalaya, Pakistan, *Geology*, *22*, 1075–1078, doi:10.1130/0091-7613(1994)022<1075:DEFASG>2.3.CO;2.

Yamaji, A. (2000), The multiple inverse method: A new technique to separate stresses from heterogeneous fault slip data, *J. Struct. Geol.*, *22*, 441–452, doi:10.1016/S0191-8141(99)00163-7.

Yamaji, A., S. Tomita, and M. Otsubo (2005), Bedding tilt test for paleostress analysis, *J. Struct. Geol.*, *27*, 161–170, doi:10.1016/j.jsg.2004.08.006.

Zanchi, A., and M. Gaetani (1994), Introduction to the geological map of the North Karakoram Terrain from the Chapursan valley to the Shimshal Pass 1:150000 scale, *Riv. Ital. Paleontol. Strat.*, *100*, 125–136.

Zanchi, A., and D. Gritti (1996), Multistage structural evolution of Northern Karakorum (Hunza region, Pakistan), *Tectonophysics*, *260*, 145–165, doi:10.1016/0040-1951(96)00081-9.

Zeilinger, G., J.-P. Burg, N. Chaudhry, H. Dawood, and S. Hussain (2000), Fault systems and paleo-stress tensors in the Indus Suture Zone (NW Pakistan).), *J. Asian Earth Sci.*, *18*(5), 547–559, doi:10.1016/S1367-9120(99)00084-X.

Zeilinger, G., D. Seward, and J.-P. Burg (2007), Exhumation across the Indus suture zone: A record of back sliding of the hanging wall, *Terra Nova*, *19*(6), 425–431, in press., doi:10.1111/j.1365-3121.2007.00767.x.

Zeitler, P. K. (1985), Cooling history of the NW Himalaya, Pakistan, *Tectonics*, *4*(1), 127–151, doi:10.1029/TC004i001p00127.

Zeitler, P. K., C. P. Chamberlain, and H. A. Smith (1993), Synchronous anatexis, metamorphism, and rapid denudation at Nanga Parbat (Pakistan Himalaya), *Geology*, *21*, 347–350, doi:10.1130/0091-7613(1993)021<0347:SAMARD>2.3.CO;2.

Zeitler, P. K., et al. (2001a), Crustal reworking at Nanga Parbat, Pakistan: Metamorphic consequences of thermal-mechanical coupling facilitated by erosion, *Tectonics*, *20*, 712–728, doi:10.1029/2000TC001243.

Zeitler, P. K., et al. (2001b), Erosion, Himalayan geodynamics, and the geomorphology of metamorphism, *GSA Today*, *11*, 4–9, doi:10.1130/1052-5173(2001)011<0004:EHGATG>2.0.CO;2.

S. Guillot, A. Pêcher, P. van der Beek, and J. Van Melle, LGCA, Université de Grenoble, CNRS, BP 53, F-38041, Grenoble, France. (arnaud.pecher@ujf-grenoble.fr)

F. Jouanne and J. L. Mugnier, Laboratoire de Géodynamique des Chaînes Alpines, Université de Savoie, Campus Scientifique, CNRS, F-73376, Le Bourget du Lac, France.

A. Kausar, M. Latif, and A. Majid, Geological Survey of Pakistan, Plot No. 84, H-8/1, Islamabad, Pakistan.

G. Mahéo, Laboratoire de Sciences de la Terre, Université de Lyon 1 et ENS de Lyon, CNRS, 2 rue R. Dubois, F-69622, Villeurbanne, France.

Y. Rolland, Géosciences Azur, UMR 6526, Université de Nice, CNRS, BP 2135, F-06103, Nice, France.

L. Seeber, Lamont-Doherty Earth Observatory, Earth Institute at Columbia University, Palisades, NY 10964, USA.